# 2

# Biomineralization and Biomimetic Synthesis of Biomineral and Nanomaterials

Ming-Guo Ma and Run-Cang Sun
*Institute of Biomass Chemistry and Technology,*
*College of Materials Science and Technology,*
*Beijing Forestry University*
*P. R. China*

## 1. Introduction

Biominerals and biomaterials with unique microstructure are mainly consisted of organic and inorganic materials, and exhibit excellent biological and mechanical properties. The formation mechanism of biomineral indicated that the organic matrixes have an important influence on the morphology and structure of the inorganic matrix material in the process of biomineralization. However, the biomineralization mechanism research of biomineral is still in the initial stage, many phenomena need to be further explored, such as the effect of organisms on the different morphologies and polymorphs of biominerals, the biomineralization mechanism of the formation process of the biomineral in the existence of organic matter. Biomineralization and biomimetic synthesis of biomineral and nanomaterials have been receiving considerable attention. Biomineralization is the formation process of mineral by organisms. Biomimetic synthesis is simulation of biomineralization, using the mechanism of biomineralization, to achieve biomineral and materials with special structure and function. In a word, biomimetic synthesis is learning from the mineralization of organisms and learning from nature. Therefore, we should understand the concepts, process, and mechanism of biomineralization, which was briefly reviewed in section one.

Biomineral including calcium phosphate, hydroxyapatite (HA), calcium silicate, calcium carbonate, and calcium sulfate, are important calcium-based inorganic biodegradable materials and have been widely used in biomedical field. Biomineralization is the mineralization of biomineral. Biomimetic synthesis was first used in the fabrication of biomineral. So it is necessary to provide an overview of the biomimetic synthesis of biomineral. This chapter summarizes our recent endeavors on the biomimetic synthesis of biomineral including HA, calcium silicate, $CaCO_3$, $BaCO_3$, and $SrCO_3$, etc.

Biomineral synthesis includes morphology, structure, and function biomineral synthesis. It is well known that the structure determines property and the morphology is the external display of structure. Here, we intend to review recent progress in biomineral synthesis of other nanomaterials.

## 2. Biomimetic synthesis of calcium-based inorganic biodegradable nanomaterials

### 2.1 Background

The biomineral in nature with different composition and specific biological functions formed from the body of bacteria, microbes, plants, and animals has more than sixty kinds of species. Among the half of the biomineral, calcium-based inorganic biodegradable nanomaterials (CIBNs) including calcium phosphate, hydroxyapatite (HA), calcium silicate, calcium carbonate, and calcium sulfate, etc, are important materials and have been widely used in biomedical fields such as bone cements (Islas-Blancas et al., 2001), drug delivery (Kim et al., 2004), tooth paste additives (Oktar et al., 1999), dental implants (Gross et al., 1998), gas sensors, ion exchange (Yasukawa et al., 2004), catalysts or catalysts supports (Venugopal & Scurrell, 2003), and host materials for lasers (Garcia-Sanz et al., 1997). Compared to biomedical polymer materials, CIBNs have received considerable attention due to their excellent osteoconductivity, biocompatibility, bioactivity, biodegradablity, chemical stability, and mechanical strength (Hing, 2004; Boskey et al., 2005; Wahl & Czernuszka, 2006; Dorozhkin, 2007). CIBNs have some solubility, bonding ability between biological tissues, releasing innoxious ions on the body and can promote repairment in tissue. However, the traditional biodegradable materials mainly refer to polymers with biodegradable ability such as poly(lactic acid) and poly(amino acid). So strengthen the research of CIBNs as the expansion of biodegradable materials will do a favor to exploiting the applications of biomedical materials.

For a long time, CIBNs have been considered as a kind of bioactivity materials. CIBNs, for example bioactive glass, bioactive cement, HA, etc, have been found to have some solution and absorption in the organism, and they had calcium and phosphorus element in their composition, which can be replaced in the body's normal metabolism pathway through the hydroxyl groups bonding to human tissue. The defect sites could be completely replaced by new bone tissue after the implantation of CIBNs, while the CIBNs were only used as temporary scaffolds. Some of CIBNs even took part in the formation of new bone. β-tricalcium phosphate (β-TCP) porous materials were fabricated by Getter et al. in 1972, and they also made use of β-TCP as bone graft in 1977 (Cameron et al., 1977), and made clinical bone fill experiment in 1978. Using β-TCP in bone regeneration experiment was first reported in 1981 (Groot & Mitchell, 1981). In recent years, it was found that β-TCP is a good tissue engineering scaffold material in biomedical field. This type of material has some advantages including the gradual degradation in the organisms' metabolic process, the process of replacement and growth of new bone, without prejudice to newly grown bone in material substitution process.

It is well known that the naturally tooth and bone are organic/inorganic composites with the ingredients including calcium phosphate, HA, calcium silicate, and calcium carbonate. Especially, HA is similar in composition to bone mineral, has been found to promote new bone formation when being implanted in a skeletal defect, and has been used in clinical bone graft procedures for about 30 years. However, its poor tensile strength and fracture toughness make it unsuitable for practical applications. It was discovered that naturally derived tooth HA did not differ from synthetic ones (Oktar et al., 1999). A nanostructured HA was thermally sprayed on Ti-6Al-4V substrates via high velocity oxy-fuel, and a uniform layer of apatite was formed via immersing the coating in a simulated body fluid (SBF) for 7 days (Lima et al., 2005). Thian *et al* (2006). fabricated nanocrystalline silicon-substituted HA thin coatings with enhanced bioactivity and biofunctionality applied to a

titanium substrate via a magnetron co-sputtering process. An increase in the attachment and growth of human osteoblast-like (HOB) cells on these coatings was observed throughout the culture period, with the formation of extracellular matrix. Biomedical nanocomposite fibers of HA/poly(lactic acid) with homogeneous structure were synthesized by electrospinning (Kim et al., 2006). Initial cellular assays indicated excellent cell attachment and proliferation.
In this section, we briefly review the interrelated papers concerning the biomimetic fabrication, mechanism, and future development of CIBNs. The chapter also provides an overview about the potential application of nanotechnology in biomedical field (Ma & Zhu, 2010).

### 2.2 Fabrication of calcium-based inorganic biodegradable nanomaterials

Some successful methods including precipitation, hydrothermal, microemulsion, sol-gel, biomimetic synthesis have been employed for the synthesis of CIBNs**.** The liquid phase precipitation method is one of the earliest methods for the synthesis of CIBNs. In recent years, the system such as $Ca(OH)_2$-$H_3PO_4$-$H_2O$, $Ca(NO_3)_2$-$NH_4NO_3$-$NH_3 \cdot H_2O$, $CaCl_2$-$K_2HPO_4$-KOH, and $CaHPO_4$-$Ca_4(PO_4)_2O$-$H_2O$ has been adopted in the preparation of HA (Tarasevich et al., 2003; Lu & Leng, 2005; Kanakis et al., 2006). However, impurities were also observed as the byproducts. Some successful strategies including chemical mechanical vapor deposition (Chi, 2010), mechano-chemical process (Tofighi & Rey, 2010), dual nozzle spray drying techniques (Chow & Sun, 2010), high alumina fly ash (Zhang et al., 2009), have been also employed for the synthesis of CIBNs.
HA and calcium silicate are the typical examples among the CIBNs. HA has a composition and structure analogous to the bone apatite and shows high bioactivity (Suchanek et al., 2002; Landi et al., 2004 ; Sun et al., 2009). Calcium silicate is used in drug delivery and bone tissue regeneration due to its good biocompatibility, bioactivity, and degradability (Matsuoka et al., 1999; Oyane et al., 2003; Cortes et al., 2004; Li & Chang, 2005; Jain et al., 2005; Kokubo et al., 2005). Recently, the key point of the present research aims to the synthesis of HA (Rudin et al., 2009) and calcium silicate nanostructures by novel methods. Liu *et al* (2005). fabricated HA nanoribbon spheres by a one-step reaction using the bioactive eggshell membrane as a directing template in the presence of ethylenediamine. The authors indicated that spheres can be modified with fluorescein to obtain a fluorescent probe material with strong luminescence. HA nanorods were formed by the liquid-solid solution method reported by Wang *et al*.(2006). The bubble-template route is also employed to synthesize flower-like porous B-type carbonated HA microspheres (Cheng et al., 2009). Using double emulsion droplets as microreactors, mesoporous HA could be fabricated (Shum et al., 2009). The size and the geometry of the droplet microreactors can be tuned by using capillary microfluidic techniques. We reported the synthesis of hierarchically nanostructured HA hollow spheres using $CaCl_2$, $NaH_2PO_4$, and potassium sodium tartrate via a solvothermal method at 200 °C for 24 h in water/*N*,*N*-dimethylformamide (DMF) mixed solvents, HA microtubes using $CaCl_2$ and $NaH_2PO_4$ in mixed solvents of water/DMF by a solvothermal method at 160 °C for 24 h (Fig. **1**) (Ma et al., 2008; Ma & Zhu, 2009).
Currently, the research of CIBNs has been focus on β-tricalcium phosphate (β-TCP), $CaSO_4$, calcium silicate, and some natural materials such as natural coral (primarily composed of $CaCO_3$) and its composite materials. These materials are mainly used in bone substitute materials, or scaffolds for tissue engineering. The drug loading and releasing materials are mostly made of the biodegradable polymers. With the development of CIBNs, their application can also be extended to controlled drug delivery system.

Using HA and calcium silicate in drug delivery and other biomedical applications has become a key topic regarding CIBNs' application. A novel magnetic HA nanoparticles can be used as non-viral vectors for the glial cell line-derived neurotrophic factor gene by the treatment with iron ions using a wet-chemical process (Wu et al., 2010). Yuan *et al* (2010). investigated the effect of the particle size of the HA nanoparticles on the anti-tumor activity, apoptosis-induction and the levels of the apoptotic signaling proteins in human hepatoma HepG2 model cells. The experiments indicated that the size of HA and thereby the cellular localization had predominant effect on the HA-induced cytotoxicity, apoptotis, and the levels of the apoptotic proteins in HepG2 cells. HA nanoparticle-coated micrometer-sized poly(L-lactic acid) microspheres were fabricated via a "Pickering-type" emulsion route in the absence of any molecular surfactants, which can promote the cell adhesion and spreading (Fujii et al., 2009).

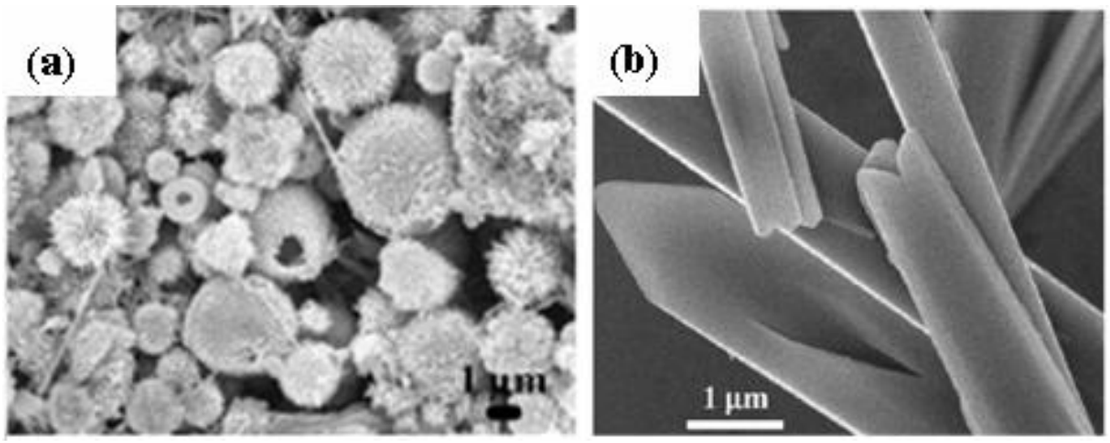


Fig. 1. (a) SEM micrograph of the hierarchically nanostructured HA hollow spheres, (Reproduced with permission from Eur. J. Inorg. Chem. **2009**, 5522. Copyright **2009** *VCH*.) and (b) TEM micrograph of the HA microtubes. (Reproduced with permission from Mater. Lett. **2008**, *62*, 1642. Copyright **2008** *Elsevier*)

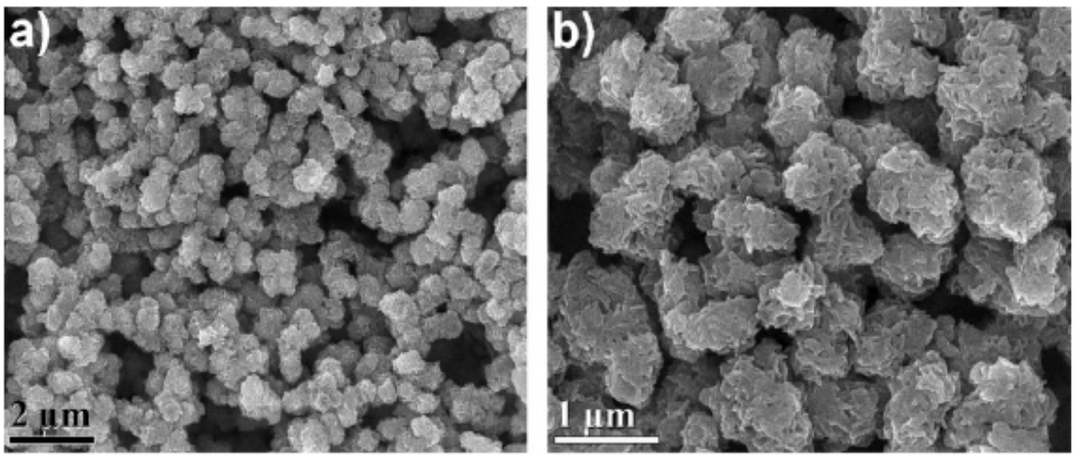


Fig. 2. SEM images of hierachically nanostructured mesoporous spheres of calcium silicate hydrate, prepared by the surfactant-free sonochemical synthesis. Reproduced with permission from Adv. Mater. **2009**, *22*, 749. Copyright **2009** *VCH*.

In the past decades, calcium silicate materials have drawn growing attention on their potential applications in the bone tissue engineering field (Rodríguez-Lorenzo et al., 2009; Wei et al., 2009). Nanosized calcium silicate and poly(epsilon-caprolactone) nanocomposite for bone tissue regeneration using calcium silicate slurry, other than dried calcium silicate powder, was fabricated by Wei *et al* (2009). in a solvent-casting method. The results suggested that the incorporation of calcium silicate could significantly improve the hydrophilicity, compressive strength, and elastic modulus of calcium silicate/poly(epsilon-caprolactone) composites.

Some studies have been carried out on calcium silicate transformation to bonelike apatite/HA, but few have extended their applications in drug delivery systems (Jain et al., 2005; Li & Chang, 2005). Recently, Wu *et al*. (2009) reported the low-cost and surfactant-free sonochemical synthesis of hierachically nanostructured mesoporous spheres of calcium silicate hydrate with well-defined 3D network structures constructed by nanosheets as building blocks (Fig. **2**). The calcium silicate hydrate has the advantages of large specific surface area, large pore volume, extremely high drug-loading capacity (2.29 g IBU is loaded in per gram carrier), adjustable drug-release rate, good bioactivity, and fine biodegradability. Moreover, calcium silicate hydrate can entirely transform to HA after the drug release in simulated body fluid, implying the good bioactivity and biodegradability. Besides the hierachically nanostructured mesoporous spheres of calcium silicate hydrate, they also prepared HA and calcium silicate nanostructured porous hollow ellipsoidal capsules, which were constructed by nanoplate networks using the inorganic $CaCO_3$ template (Fig. **3**) (Ma et al., 2008). $CaCO_3$ ellipsoids were synthesized via the reaction between $Ca(CH_3COO)_2$ and $NaHCO_3$ in water and ethylene glycol mixed solvent at room temperature. The drug loading and release behavior of HA hollow capsules indicated that HA hollow capsules had a high specific surface area and high storage capacity. Calcium phosphate (CaP)/PLGA-mPEG hybrid porous nanospheres were synthesized by a facile room-temperature method, which can be applied as DNA vectors for DNA loading and in vitro transfection (Wang et al., 2010).

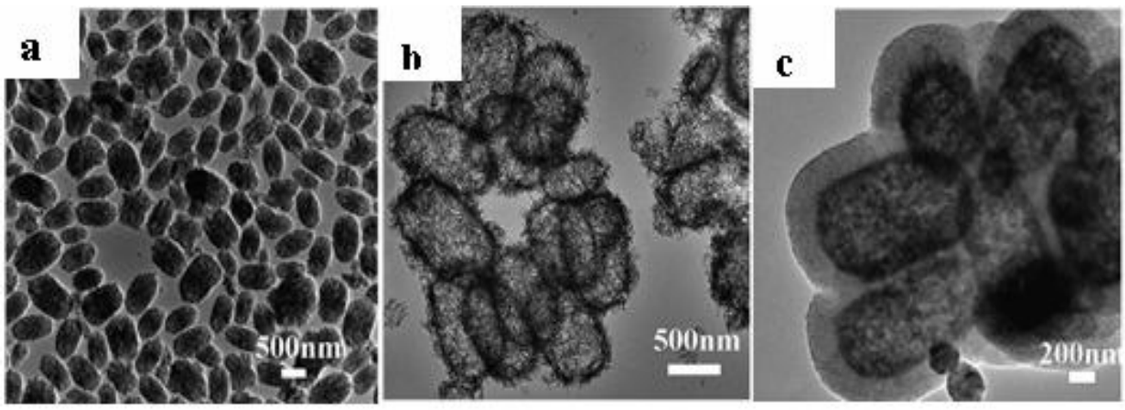


Fig. 3. TEM micrographs of (a) $CaCO_3$ cores, (b) HA nanostructured hollow ellipsoidal capsules, (c) calcium silicate nanostructured hollow ellipsoidal capsules. Reproduced with permission from J. Mater. Chem., **2008**, *18*, 2722. Copyright **2008** *RSC*.

In addition, the synthesis of calcium phosphate (Lee et al.,2009; Matsumoto & Nakasu,2010)., dipterinyl calcium pentahydrate (Moheno & Pfleiderer, 2010), calcium phosphate pasty material (Lacout et al., 2009), and HA calcium phosphates (Godber & Leite, 2009) has been also reported. Calcium sulfate was aseptic, biocompatible and biodegradable,

which was an ideal substitute of bone transplantation material (Mirtchi et al., 1990; Sato et al., 1998; Nilsson et al., 2002; Bohner, 2004), and antibiotic-carrier material (McKee et al., 2002; Rauschmann et al., 2005).

A single component of CIBNs has some limitations such as too fast or too slow degradation time, low mechanical properties. However, compared to the individual components, nanocomposites provided the possibility for the enhancement of multifunctional properties due to interaction between the counterparts. Therefore, to develop new CIBNs-based nanocomposites with the control over the crystal phase and morphology is of great importance for broadening applications of CIBNs.

There are a few reports about CIBNs-based nanocomposites (Sotome et al., 2009; Furuzono et al., 2009; Yaszemski et al., 2010). Chitosan-HA nanostructured biocomposite films with high volume fraction were prepared by solvent casting their hybrid suspensions using biomimetic synthesis method (Kithva et al., 2010). HA-coated zirconia-magnesia composite for protein separation was also be prepared by biomimetic technique (Li & Feng, 2009). An invention patented by Ding *et al*. (2009) has provided a sol-gel method for synthesizing calcium silicate-based composite cement, which provided a novel mixture for bone tissue repairment. Bioactive bone-repairing materials with mechanical properties analogous to those of natural bone can also be fabricated through the combination of calcium silicate with polyetheretherketone (Kim et al., 2009).

As the most abundant renewable material and natural polysaccharide found on earth, cellulose becomes one of important biodegradable materials owing to its unique properties such as chemical stability, mechanical strength, biocompatibility, biodegradation (Iguchi et al., 2000; Gindl & Keckes, 2004; Shoda & Sugano,2005). The cellulose-calcium silicate nanocomposites are considered to have potential applications in biomedical field with such striking features as high mechanical properties and excellent biocompatibility. We fabricated the cellulose-calcium silicate nanocomposites with calcium silicate nanoparticles homogeneously dispersed in the cellulose matrix using cellulose solution, $Ca(NO_3)_2{\cdot}4H_2O$ and $Na_2SiO_3{\cdot}9H_2O$ in ethanol/water mixed solvents at room temperature for 24 h (Fig. **4a**) (Li et al., 2010). Cellulose-HA nanocomposites were also obtained using microcrystalline cellulose, $CaCl_2$, and $NaH_2PO_4$ in *N*,*N*-dimethylacetamide solvent by microwave-assisted method at 150 °C (Fig. **4b**) (Ma et al., 2010).

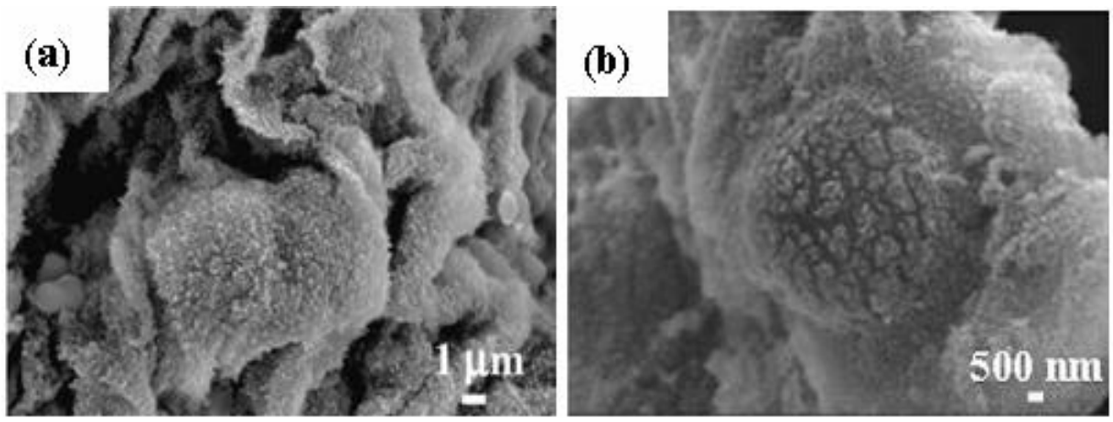


Fig. 4. SEM micrographs of (a) the cellulose-calcium silicate nanocomposites and (b) the cellulose-HA nanocomposites. Reproduced with permission from Carbohydr. Polym. **2010**, *80*, 270 and Carbohydr. Res., **2010**, *345*, 1046. Copyright **2010** *Elsevier*.

In view of the recently research of the fabrication of CIBNs and CIBNs-based nanocomposites, development of simple, low-cost, and high yield methods for the synthesis of CIBNs with complex microstructure and complex components is of great importance for broadening and improving their industrial applications. For example, one can combine the advantages of two or more kind's methods such as sol-gel-hydrothermal, microwave-hydrothermal, electrospinning-hydrothermal methods to fabricate CIBNs. The CIBNs with hierarchically nanostructure and/or pore microstructure have high surface area and can be promisingly used in biomedical fields. It is worth pointing out that the main challenge associated with making effective and functional nanocomponents of CIBNs is related to their homogeneous dispersion within a polymer matrix. Although rapid progress has been made in the past years, the strategies for the fabrication of CIBNs-based nanocomposites need to be further explored.

### 2.3 Degradation mechanism of calcium-based inorganic biodegradable nanomaterials

The degradation of CIBNs had two routes: the dissolution by body fluids, and phagocytosis and absorption by cells (mainly macrophage), except that calcium sulfate was relatively easy to dissolve in the body. As fluid contained a number of acidic metabolites such as citrate, lactate and acid hydrolysis enzyme in the implants, which provided acidic environment for dissolution of the material, CIBNs were split into particles, molecular or ion. The degradation process of macrophages on CIBNs can be divided into intracellular and extracellular degradation.

Particles were split into ions after phagocytosis by macrophages under the effect of cytoplasmic and lysosomal enzymes, and then the degradation products such as $Ca^{2+}$, $PO_4^{3-}$, $CO_3^{2-}$, $SO_4^{2-}$, etc, can be transferred to extracell. In addition, macrophages contained rich acid hydrolase including lysosomal enzyme and acid phosphatase enzymes, which can secrete $H^+$ to the area of extracell and induce the formation of acidic environment. If the diameter of β-TCP particles was bigger than the size of macrophages (14~20 μm), macrophages may extend small protuberances, covering and closely attaching to their surface, and forming a closed cell-material area. At the same time, the dissolved enzyme of cytoplasm of macrophages can release in this areas. The $CO_2$ and $H_2O$ in macrophages form carbonate under the action of carbonic anhydrase, and then decomposed into $HCO_3^-$ and $H^+$. $H^+$ induced the high-acid environment at cell-material area, which cause the degradation of β-TCP particles. For example, the extracellular degradation process of calcium phosphate can be expressed by the following formula:

$$CO_2 + H_2O \xrightarrow{CA} H_2CO_3 \xrightarrow{CA} H^+ + HCO_3^-$$

$$Ca_3(PO_4)_2 \xrightarrow{H^+} Ca^{2+} + 2CaHPO_4 \xrightarrow{H^+} 3Ca^{2+} + 2PO_4^{3-}$$

The degradation product, $Ca^{2+}$, can enter the blood through the blood circulation to the organs and tissues, to participate in metabolism, and be excreted through feces and urine from liver and kidneys. The other part is stored and used when needed, without causing organic damage and pathological tissue calcification. The CIBNs can be degraded and absorbed. Its metabolites can participate in the formation of new bone, thus completing the transform from inorganic materials to organism.

The considerable changes of the HA implants displayed in surface morphology caused by leaching, corrosion, and active resorption by osteoclasts cells was reported in 1990 by Muller-Mai *et al*. (1990) using scanning electron microscopy (SEM) and transmission electron microscopy (TEM) tracking transverse fractures in the interface. The effect of osteoclasts cells on the degradation mechanism of CIBNs was further research by Wenisch *et al*, (2003) who reported that osteoclasts were localized immediately beneath the ceramic surface after 6 weeks of implantation by simultaneous resorption and phagocytosis, and were capable of phagocytosing the resorbed CaP crystals. Recently, the effect of osteoclastic sodium-bicarbonate co-transporter (NBCn1) on the degradation of HA was investigated in vivo and in vitro (Riihonen et al., 2010). They discovered that down regulation of NBCn1 both on mRNA and protein level inhibited bone resorption and increased intracellular acidification in osteoclasts.

The bone formation around HA blocks was observed by using HA as a space filler in surgically created bone defects of seven cases due to curettage of bone tumours or removal for bone grafts (Yamaguchi et al., 1995). After that, the differences of bone bonding ability and degradation behaviour in vivo were observed between amorphous calcium phosphate (ACP) and highly crystalline HA coating by implantation in the tibiae of rabbits and rats (Nagano et al., 1996). The HA coating benefits to coating longevity, while the ACP coating may be in favor of the osteoconducive property of calcium phosphate coating for initial fixation of porous materials. The ratio of crystalline and amorphous contents also has an effect on the degradation (Gross et al., 2002). A high amorphous content provides fast resorption, while the amount of crystalline particles increased at the distal location of the stem and the threads of the acetabular shell. The Ca/P ratio is another important key factor (Wang et al., 2003). It was indicated that the relatively small amount of CaO was more susceptible to degradation and the TCP-containing ceramic exhibited slightly higher resistance to degradation than HA. The HA-coated AZ31 alloy with good bioactivity, which was prepared by a cathodic electrodeposition method and post-treated with hot alkali solution (Wen et al., 2009), slowed down the degradation rate and effectively induced the deposition of Ca-P-Mg apatite in simulated body fluid (SBF).

The intrinsic mechanism of CIBNs needs to be further explored due to the complexity of biochemistry process. Deep understanding of the degradation mechanism can instruct the synthesis of CIBNs and improve the applications of CIBNs. The intrinsic degradation mechanism will be gradually discovered with increased level of awareness and testing technology.

## 2.4 Current & future developments

In recent years, rapid progress has been made in the preparation of CIBNs nanostructures, the understanding of mechanism of CIBNs, and exploration of their extensive biomedical applications. So far, inorganic biodegradable materials have been widely used for bone or bone substitute materials, dental filling materials, scaffold materials for temporarily replacing injured skeleton and promoting new tissue formation. However, the practical application research of CIBNs has just started; therefore there are many unknown things that need to be explored, such as the interaction mechanism of inorganic nanoparticles and cancer cells, the biological effects from nanoparticles, and so on. Using nanoparticles in cell separation, cell staining, special drugs and new antibodies for the locally oriented therapy is currently in the initial stage.

Using biodegradable nanomaterials as carrier material in drug delivery system is still limited to organic biomaterial. There have been only a few reports using CIBNs as drug delivery carrier materials. These new fields need to be explored. For example, radiation therapy is a useful method for the cancer surgery, but at the same time a large area of radiation will harm normal cells, especially the bone marrow stem cells with the hematopoietic and immune function. The research discovered that apatite nanoparticles can inhibit a variety of cancer cells and has promising potential applications in various fields. HA nanoparticles had no effect on normal cell activity in cell culture experiments in 1992 (Li et al., 1992). HA crystallite can inhibit the growth of cancer cells in 1994 (Kano et al., 1994). It was found that the cytosolic $Ca^{2+}$ concentration of W-256 carcinosarcoma cells increased under HA microcrystals. Sakai *et al.* (1994) also reported the $Ca^{2+}$ concentration of tumor cells increased in the experiments of photo-excitation $TiO_2$ nanoparticles. It indicated the death of tumor cell because of important physiological functions of $Ca^{2+}$ on the cells. Of course, the intrinsic and detailed restraining mechanism of $Ca^{2+}$ to cancer cell growth needs to be further explored.

In addition, the fast development of tissue engineering brings forward high requirements on biomedical materials. CIBNs adapt to the standard of biomedical applications. CIBNs can be gradually degraded or dissolved under physiological condition, and was absorbed by the body metabolism. Moreover, the units or their degradation products of the majority composition of CIBNs are small molecules or ions in vivo and have good biocompatibility and safety, compared to non-degradable material.

## 3. Biomimetic synthesis of $CaCO_3$, $BaCO_3$, $SrCO_3$ and $BaCrO_4$

$CaCO_3$ is a typical biomineral that is abundant in both organisms and nature and has important industrial applications. $CaCO_3$ has six polymorphs: vaterite, aragonite, calcite, amorphous, crystalline monohydrate, and hexahydrate $CaCO_3$ (McGrath, 2001). Therefore, to develop new synthesis methods for the control over the crystal phase and morphology are of great importance for broadening applications of $CaCO_3$. Moreover, $CaCO_3$ is sensitive to the synthesic condition. The biomimetic synthesis of $CaCO_3$ with various unusual biomimetic morphologies, such as pumpkin-like, olive-like, sphere–like, willow-leaf-like, flower-like, cauliflower-like, polyhedron-like, etc, was reported by one-step base- and microwave-assisted method using $CaCl_2$, $(NH_4)_2CO_3$ or $Na_2CO_3$, basic additives (urea, hexamethylenetetramine ($(CH_2)_6N_4$, HMT), ethylenediamine ($C_2H_8N_2$, EDA) and NaOH), poly(vinylpyrrolidone) (PVP)) in a polyol solvent (Fig. 5) (Ma et al., 2010). The experimental results indicated that the heating temperature, heating time and the type of the basic additive has significant effects on the morphology and the polymorph of $CaCO_3$ crystals. This microwave-assisted heating method is simple, fast, low-cost and may be scaled up for large-scale production of $CaCO_3$ with various unique morphologies.

Using $(NH_4)_2CO_3$ without any basic additive at 130 $^oC$, the pumpkin-like morphology of aragonite with sizes of about 1 μm (Fig. 5a). The low magnification view of SEM in Fig. 5a shows relatively uniform sizes of pumpkin-like aragonite. The insets of Fig. 5a show typical aragonite pumpkins at high magnification. Each pumpkin-like microstructure consisted usually of four parts (the right-upper inset of Fig. 5a), and was open at both ends (the left-bottom inset of Fig. 5a).When $Na_2CO_3$ was used instead of $(NH_4)_2CO_3$ as the $CO_3^{2-}$ source and without any basic additive at 130 $^oC$, the shape of $CaCO_3$ was irregular instead of the pumpkin-like morphology in the case of $(NH_4)_2CO_3$. Even when the temperature was increased to 180 $^oC$, the shape of $CaCO_3$ was still irregular (Fig. 5b). In this case, the main

phase of $CaCO_3$ prepared was calcite, other than aragonite in the case of $(NH_4)_2CO_3$. From Fig. 5b, some irregular cube-like morphologies, which are typical morphologies for the calcite phase. The different results obtained by using $Na_2CO_3$ and $(NH_4)_2CO_3$ may be due to the different pH of the solution. $Na_2CO_3$ is more basic than $(NH_4)_2CO_3$.

The $CaCO_3$ prepared using $(NH_4)_2CO_3$ and urea at 150 $^oC$ consisted mainly of crystalline aragonite phase with an olive-like morphology (Fig. 5c). The inset of Fig. 5c shows a typical olive-like morphology at a high magnification. We also carried out the preparation at 180 $^oC$, however, no product was obtained. This was due to the decomposition of $(NH_4)_2CO_3$ at 180 $^oC$. The olive-like morphology was formed by the assembly of $CaCO_3$ nanoparticles. If $Na_2CO_3$ and urea were used at 180 $^oC$, the sample prepared consisted mainly of aragonite with the porous willow-leaf-like morphology (Fig. 5d). Cross-willow-leaf-like morphology was also observed. This porous willow-leaf-like morphology of aragonite prepared by the present method is quite different from the spherulite morphology of vaterite prepared using $CaCl_2 \cdot 2H_2O$ and urea in a polyol solvent under solvothermal condition (Li et al., 2002) and also different from the needle-like aragonite prepared by aging the solution of $CaCl_2$ in the presence of urea in ultrasonic bath at 90°C (Wang et al., 1999).

When using $(NH_4)_2CO_3$ and hexamethylenetetramine as a basic additive, $CaCO_3$ spheres assembled from nanoparticles of the vaterite phase were formed (Fig. 5e). The inset of Fig. 5e shows a typical sphere with the diameter of about 600 nm. If $Na_2CO_3$ instead of $(NH_4)_2CO_3$ was used, the cuboid-like morphology of calcite was obtained (Fig. 5f). When ethylenediamine was used as an additive, spherical nanoparticles of amorphous $CaCO_3$ were obtained using $(NH_4)_2CO_3$ as the $CO_3^{2-}$ source (Fig. 5g). Using $Na_2CO_3$ instead of $(NH_4)_2CO_3$ as the $CO_3^{2-}$ source and ethylenediamine, one can see the flower-like morphology of aragonite (Fig. 5h). It is well known that the ethylenediamine is a bidentate ligand and the strong coordination ability. $NH_4^+$ ions may have an influence on the coordination between ethylenediamine and $Ca^{2+}$. When a strong alkali NaOH was used instead of a weak base such as urea, hexamethylenetetramine and ethylenediamine, different morphologies were obtained. The flake congeries of vaterite were obtained using $(NH_4)_2CO_3$ as the $CO_3^{2-}$ source (Fig. 5i). Kojima et al. (1993) reported the formation of spherical vaterite by dipping spherical particles of amorphous $CaCO_3$ in $NH_4Cl$ aqueous solution, the spherical amorphous $CaCO_3$ was synthesized in the reaction system of $CaCl_2$-$Na_2CO_3$-NaOH. This indicates that $NH_4^+$ ions favor the formation of the vaterite phase. Using $Na_2CO_3$ as the $CO_3^{2-}$ source and NaOH, the cauliflower-like morphology of calcite was obtained (Fig.5j). The morphology and polymorph of $CaCO_3$ obtained by the present method is completely different from the previous reports by Kojima et al. (1993) and by Koga et al. (1998), who prepared amorphous $CaCO_3$ through reacting a mixed solution of $Na_2CO_3$-NaOH with a $CaCl_2$ solution at room temperature, respectively. From the above discussions, one can see that there is a tendency to form spherical or near-spherical morphology when using $(NH_4)_2CO_3$ as the $CO_3^{2-}$ source. When the basicity of the basic additive increases, the sizes of $CaCO_3$ structures decrease. However, there seems a tendency to form assembled complex morphology when using $Na_2CO_3$ as the $CO_3^{2-}$ source. There results shows that the source of carbonates has a significant influence on the morphology of $CaCO_3$.

When using $Na_2CO_3$ as the $CO_3^{2-}$ source and NaOH as an alkali additive by microwave heating at 180 $^oC$ for 20 min in 1,4-butanediol instead of EG, a completely different shape (polyhedral) of $CaCO_3$ was observed. In comparison, as discussed above, cauliflower-like shape was formed when using ethylene glycol as a solvent. These results indicate that the polyol solvent played an important role in the control of the morphology of $CaCO_3$.

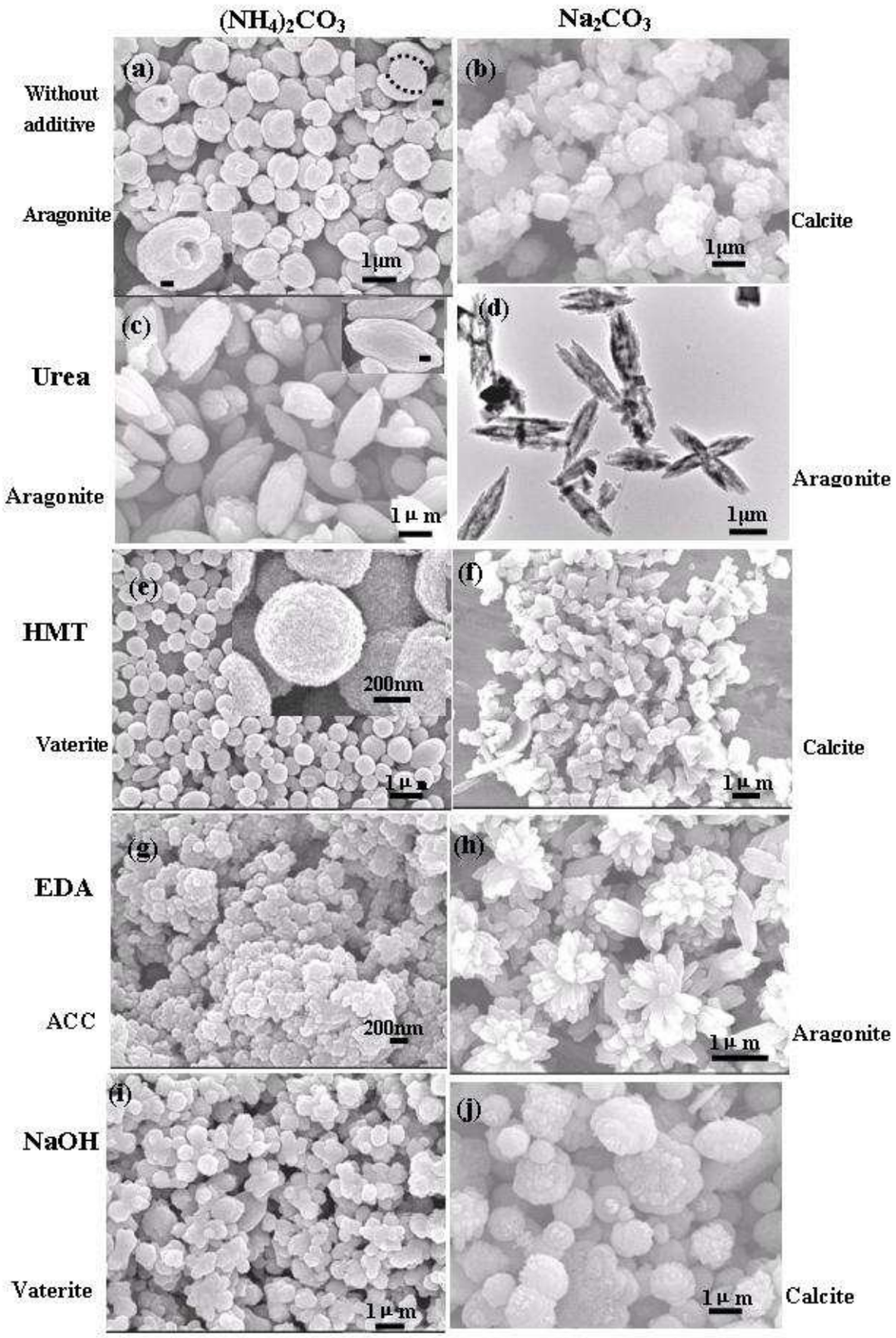
(NH4)2CO3
Na2CO3
Without additive
Aragonite
Calcite
Urea
Aragonite
Aragonite
HMT
Vaterite
Calcite
EDA
ACC
Aragonite
NaOH
Vaterite
Calcite
(a)
(b)
(c)
(d)
(e)
(f)
(g)
(h)
(i)
(j)
1μm
200nm
1μm

Fig. 5. SEM micrographs of samples prepared using different $CO_3^{2-}$ source and basic additive in EG by microwave heating for 20 min (except (j) for 1 h). (a,c,e,g,i) using $(NH_4)_2CO_3$ as the $CO_3^{2-}$ source at 130 °C (except (c) at 150 °C); (b,d,f,h,j) using $Na_2CO_3$ as the $CO_3^{2-}$ source at 180 °C. (a,b) without an basic additive, (a) shows pumpkin-like morphology of aragonite phase of $CaCO_3$, the insets of (a) show typical pumpkin-like morphology, scale bar = 200 nm, (b) shows cuboid-like morphology of calcite phase; (c,d) using urea, (c) shows a typical olive-like morphology of the aragonite phase, the inset of (c) shows a typical olive-like morphology, scale bar = 200 nm, (d) TEM micrograph showing the porous willow-leaf-like morphology of the aragonite phase; (e,f) using hexamethylenetetramine (HMT), (e) shows a sphere-like morphology assembled from nanoparticles of the vaterite phase, the inset of (e) shows a typical assembled sphere, (f) shows cuboid-like morphology of calcite; (g,h) using ethylenediamine (EDA), (g) shows spherical nanoparticles of amorphous phase of $CaCO_3$, (h) shows flower-like morphology of aragonite; (i,j) using NaOH, (i) shows the flake congeries of the vaterite phase, (j) shows cauliflower-like morphology of the calcite phase. Reproduced with permission from Adv. Mater. Res. **2010**, *92*, 139. Copyright **2010** *TTP*.

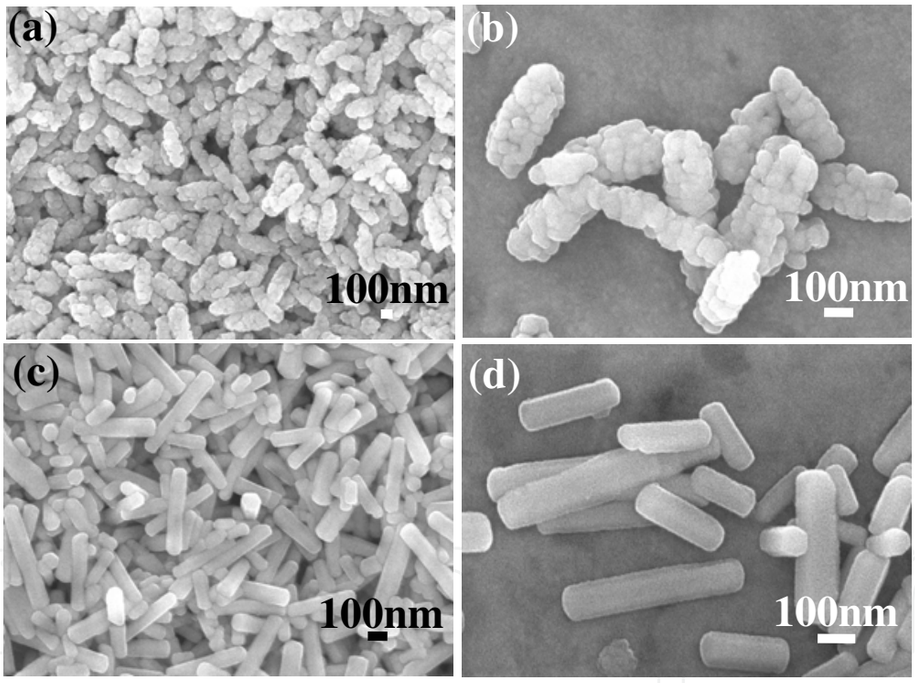


Fig. 6. SEM micrographs of $BaCO_3$ prepared by microwave heating at 90 °C for 40 min in ethylene glycol. (a,b) using NaOH, (c,d) using hexamethylenetetramine. Reproduced with permission from Chem. Lett. **2006**, *35*, 1138. Copyright **2006** *CSJ*

The above experimeatl results implied that the various basic additives and the temperature provide more possibilities for the control over the morphology and the polymorph of $CaCO_3$. However, the intrinsic and detailed biomimetic formation mechanism of $CaCO_3$ with various unusual biomimetic morphologies needs to be further explored.

Barium carbonate ($BaCO_3$) is an important material used in the production of glasses and ceramics industry (Gutmann & Chalup, 2000). $BaCO_3$ nanorods (Ma et al., 2006) can be

synthesized by the microwave-assisted method using $Ba(NO_3)_2$ and $(NH_4)_2CO_3$ in the presence of NaOH or hexamethylenetetramine ($(CH_2)_6N_4$) in ethylene glycol (Fig. 6). Fig. 6a,b shows SEM micrograph of the sample synthesized by microwave heating in the presence of a strong alkali NaOH at 90 °C for 40 min in ethylene glycol, from which one can see $BaCO_3$ nanorods assembled from nanoparticles. $BaCO_3$ nanorods had relatively uniform sizes with the diameters of about 200 nm and the lengths of about 450 nm. The influence of the weak alkalescent additive (hexamethylenetetramine) on the morphology of $BaCO_3$ was also investigated (Fig. 6c,d), from which one can see nanorods with a hexagonal cross section. This indicates that the base has a significant influence on the morphology of $BaCO_3$. $BaCO_3$ nanoparticles formed and selfassembled into nanorods in the presence of a strong basic NaOH. However, nanorods with a hexagonal cross section were obtained when using a weak basic hexamethylenetetramine.

The heating method also had an influence on the morphology of $BaCO_3$. The aggregates of irregular nanoparticles were formed in the presence of NaOH by heating in an oil bath, in contrast to the nanorods assembled from $BaCO_3$ nanoparticles prepared by the microwave heating. However, the needles with two sharp ends were produced in the presence of hexamethylenetetramine by heating in the oil bath.

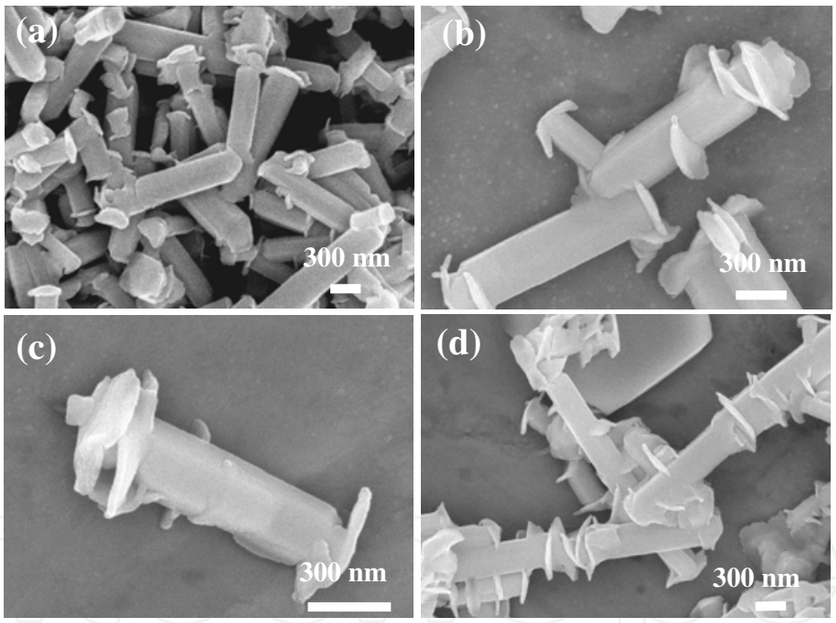


Fig. 7. SEM micrographs of $BaCO_3$. Reproduced with permission from Mater. Lett. **2007**, *61*, 5133. Copyright **2007** *Elsevier*.

However, Barium carbonate ($BaCO_3$) nanorods (Ma et al., 2007) with the nanosheets grew perpendicularly on the nanorods were synthesized using $Ba(NO_3)_2$ and $(NH_4)_2CO_3$ in the water/ethylene glycol (EG) mixed solvents by oil bath heating at 80 °C for 30 min (Fig. 7). The molar ratio of water to EG had an effect on the morphology of $BaCO_3$. $BaCO_3$ nanorods with diameters of about 250 nm and lengths of about 1μm. It is interesting that the nanosheets grew perpendicularly on the nanorods, as shown in Fig. 7b–d. The sizes of $BaCO_3$ nanorods were relatively uniform. In contrast, the aggregates of irregular nanoparticles were formed using a basic additive sodium hydroxide in a single solvent of ethylene glycol.

The liquid phase precipitation method is one of the earliest methods for the synthesis of inorganic particles. Lamer et al. (1950) reported the synthesis of monodisperse colloidal sulfur in ethanol/water mixed solvents in 1950. The precipitation reactions involve the nucleation, growth, ripening, or agglomeration processes. The separation of nucleation and growth is the key step for the preparation of high quality crystals. The growth mechanism, such as Ostwald ripening (Dadyburjor & Ruckenstein, 1977; Sugimoto, 1978; Marqusee & Ross, 1983) and aggregation especially oriented attachment (Penn & Banfield, 1999; Banfield, 2000), will dramatically affect the size, morphology, and properties of the products. In Ostwald ripening process, the larger particles will grow at the expense of the smaller ones. The "oriented attachment" mechanism was reported by Penn and Banfield (Penn & Banfield, 1999; Banfield, 2000). Although some theories have been established, it is necessary to provide more experimental examples for better understanding of these mechanisms. $BaCO_3$ rods with diameters of about 250 nm and lengths of about several micrometers (Ma et al., 2008) were obtained using $Ba(NO_3)_2$ and $NaHCO_3$ as the $CO_3^{2-}$ source at room temperature in water (20 mL) for 30 min (Fig.8). Fig. 8a-c shows TEM micrographs of the sample using $NaHCO_3$ as the $CO_3^{2-}$ source, from which one can see $BaCO_3$ rods with diameters of about 250 nm and lengths of about several micrometers. Fig. 8b shows a typical individual nanorod. The corresponding SAED pattern of an individual rod (the up inset of Fig. 8b) indicates the single-crystalline structure of the rod, which shows that the preferential growth direction of the nanorod was along the [100] zone axis of $BaCO_3$. We also found that $BaCO_3$ rods were not stable under electron beam irradiation and changed from single crystalline to polycrystalline structure after exposure to the electron beam (the down inset of Fig. 8b). A similar phenomenon that one-dimensional structures changed under electron beam irradiation was reported for $PbCrO_4$ rods (Wang & Zhu, 2005), $Ag_6Mo_{10}O_{33}$ rods (Cui et al., 2004), and Bi nanotubes (Li et al., 2001). They all could transform into polycrystalline structure under electron beam irradiation.

It is interesting that the rod assembled from nanoparticles was observed in a few cases, as shown in Fig. 8c. One can clearly observe the nanoparticles and the boundary between the particles. The corresponding SAED pattern of the rod indicates the oriented aggregation of nanoparticles (the inset of Fig.8c), implying that the growth of $BaCO_3$ rods followed the oriented attachment mechanism. It is possible that this polycrystalline rod was an intermediate product. The oriented attachment-based self-assembly and crystallization were also reported for ZnO (Pacholski et al. 2002) and $CaCO_3$ (Zhan et al., 2003). The understanding of the formation mechanism is the key point for the realization of controlled synthesis of one-dimensional nanomaterials.

In order to understand the formation mechanism of $BaCO_3$ rods, the sample was synthesized at room temperature for 30 s, while the other reaction conditions were the same (Fig. 8d-h). All the rods were assembled from nanoparticles. A typical single rod assembled from nanoparticles was shown in Fig.8h. This result conformed that the growth of $BaCO_3$ rods followed the oriented attachment mechanism.

When using $(NH_4)_2CO_3$ as the $CO_3^{2-}$ source, a completely different shape (bundle and flower) of $BaCO_3$ was observed (Fig. 9a-b). These $BaCO_3$ bundles and flowers were assembled from nanosheets. We also investigated the effect of the surfactant on the morphology of $BaCO_3$. When P123 was used, more dense flowers were observed (Fig.9c) compared with those shown in Fig. 9a-b. When SDBS was used (Fig.9d-e), the major morphology was bundle-like, and some fragments were also observed as a minor morphology. When CTAB was used, the loosely assembled flowers were obtained (Fig. 9f). Therefore, the type of the surfactant has an effect on the morphology of $BaCO_3$.

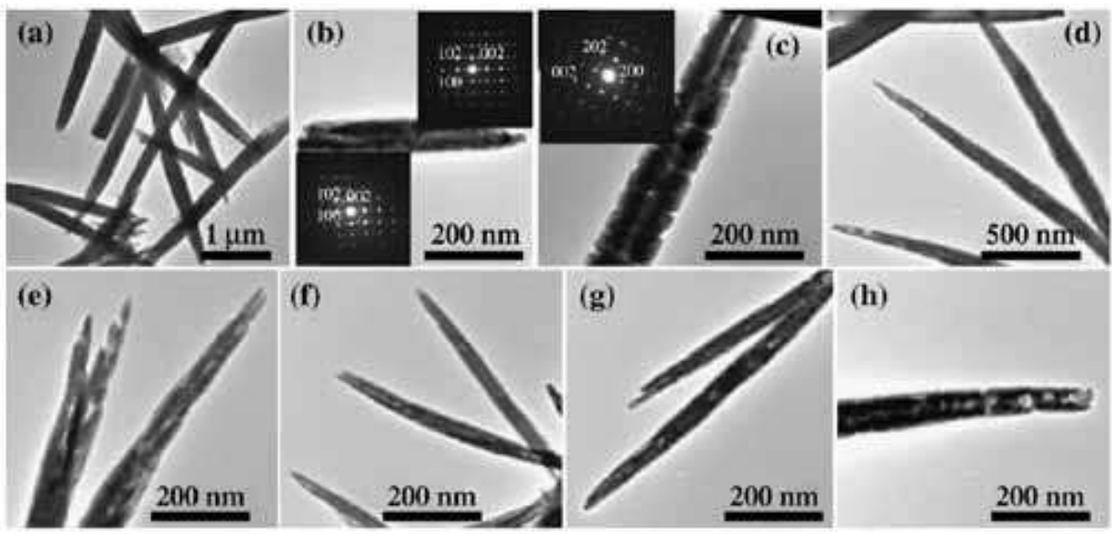


Fig. 8. TEM micrographs of the sample prepared using $NaHCO_3$ as the $CO_3^{2-}$ source for different time: (a-c) 30 min; (a) A typical TEM micrograph; (b) an individual nanorod and the corresponding SAED pattern of the individual nanorod before and after exposure to electron beam irradiation, respectively; (c) the rod assembled from nanoparticles and the corresponding SAED pattern. (d-h) 30 s. Reproduced with permission from Mater. Lett. 2008, *62*, 3110. Copyright 2008 *Elsevier*.

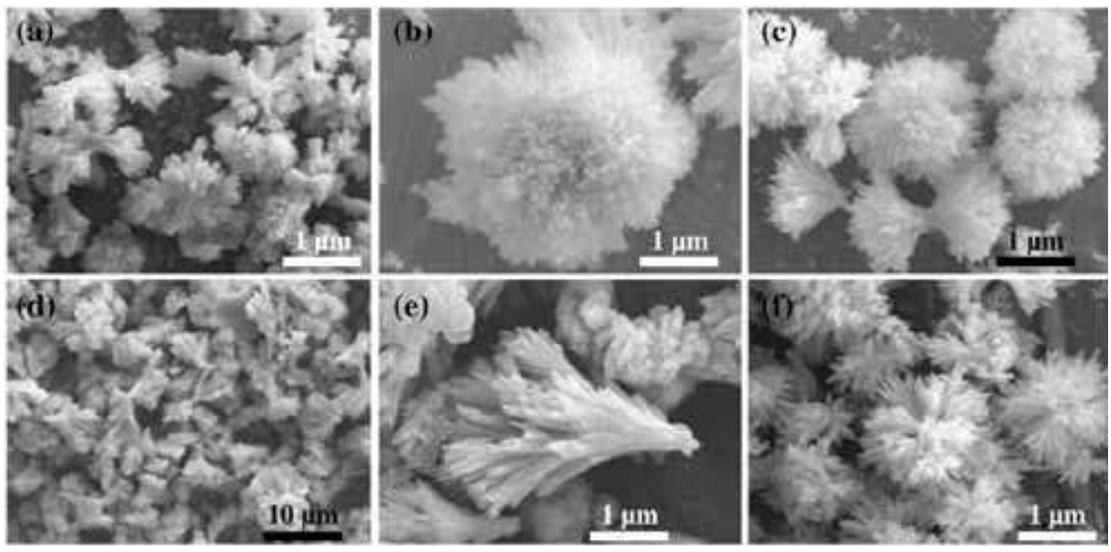


Fig. 9. SEM micrographs of the sample prepared using $(NH_4)_2CO_3$ as the $CO_3^{2-}$ source. (a) A typical SEM micrograph; (b) an individual flower-like structure. (c) using 20 mL 2.9 g/L P123; (d, e) using 20 mL SDBS (25.090 g/L); (f) using 20 mL CTAB (9.100 g/L). Reproduced with permission from Mater. Lett. **2008**, *62*, 3110. Copyright **2008** *Elsevier*.

$SrCO_3$ is a simple mineral that has only one polymorph, the study of crystallization process of $SrCO_3$ may be useful to help understand the formation of the isostructural $CaCO_3$ phase (aragonite) and the mineralization process of other biominerals. $SrCO_3$ is an important reactant in the production of glass for color television tubes and ferrite magnets for small

DC motors (Bastow, 2002), and also used in the production of iridescent and special glasses, pigments, driers, paints, pyrotechnics, catalysts and chemical sensors (Zeller, 1981; Griffiths, 1985; Erdemoğlu & Canbazoğlu, 1998; Owusu & Litz, 2000; Shi et al., 2002).

The microwave-assisted method was also used for the synthesis of $SrCO_3$ with an olive-like or flower-like morphology (Ma & Zhu, 2007) using $Sr(NO_3)_2$ and $(NH_4)_2CO_3$ in ethylene glycol or water. The olive-like morphology was obtained in ethylene glycol (Fig.10). From Fig. 10c one can see that the olive-like $SrCO_3$ structures were formed by the assembly of $SrCO_3$ nanoparticles. The sizes of olive-like $SrCO_3$ were relatively uniform. The width of the olive-like structures was about 160 nm and the length was about 500 nm. However, the flower-like (majority) and bundle-like (minority) morphology was prepared using water as the solvent instead of ethylene glycol (Fig. 11). Each flower-like or bundle-like microstructure was formed by the assembly of nanosheets. Interestingly, a hollow was observed in the central bottom of the flower-like morphology (Fig. 11c). Figs. 11b and 11c show the typical flower-like morphology of $SrCO_3$. Fig. 11e shows a typical bundle-like $SrCO_3$ assembled from nanosheets.

The heating time has an effect on the morphology of $SrCO_3$. When the heating time was 30 s (Fig. 12a), low-symmetry bundle-like $SrCO_3$ structures were observed as a major morphology and the degree of assembly was low. Flower-like morphology was formed as a minor product. When the heating time was increased to 1 min, the flower-like morphology consisted of nanosheets dominated although some bundles still existed (Fig. 12b).

It is well known that ethylenediamine is widely used as a chelating ligand in inorganic chemistry and coordination chemistry (Cotton et al., 1999). The syntheses of II-VI semiconductor 1-D nanostructures by a solvothermal process using ethylenediamine as a coordination molecular template have been reported (Gao et al., 2002). The influence of EDA on the formation of $CaCO_3$ in various reaction systems were reported (Sugihara et al., 1997). One-dimensional $SrCO_3$ nanostructures assembled from nanocrystals (Ma & Zhu, 2008) can be successfully synthesized by a microwave-assisted aqueous solution method at 90 $^oC$ using $Sr(NO_3)_2$, $(NH_4)_2CO_3$ and ethylenediamine ($C_2H_8N_2$) for 20 min (Fig. 13). When the microwave heating time was 5 min, the hexagonal cone-like structures of $SrCO_3$ were observed as majority morphology and some nanoparticles as a minor morphology were also observed (Fig. 14). Fig. 14b shows some nanoparticles surrounding the hexagonal cones. Fig. 14c shows the top view of the hexagonal cone, from which one can clearly see the six crystal planes. A typical hexagonal cone is shown in Fig. 14d, from which one can see hexagonal cylinder with cones at two ends.

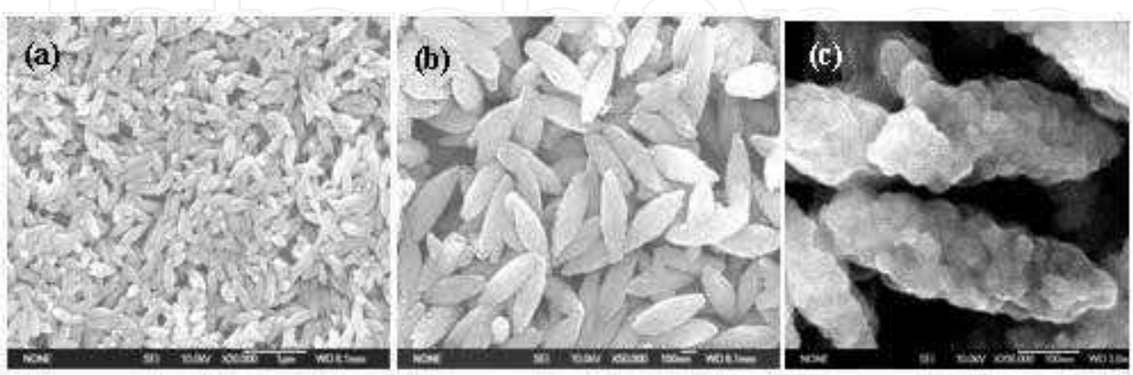


Fig. 10. SEM micrographs of $SrCO_3$ prepared using $(NH_4)_2CO_3$ and $Sr(NO_3)_2$ by microwave heating at 90 $^oC$ for 5 min in ethylene glycol. Reproduced with permission from J. Nanosci. Nanotechnol. 2007, *7*, 4552. Copyright 2007 *ASP*.

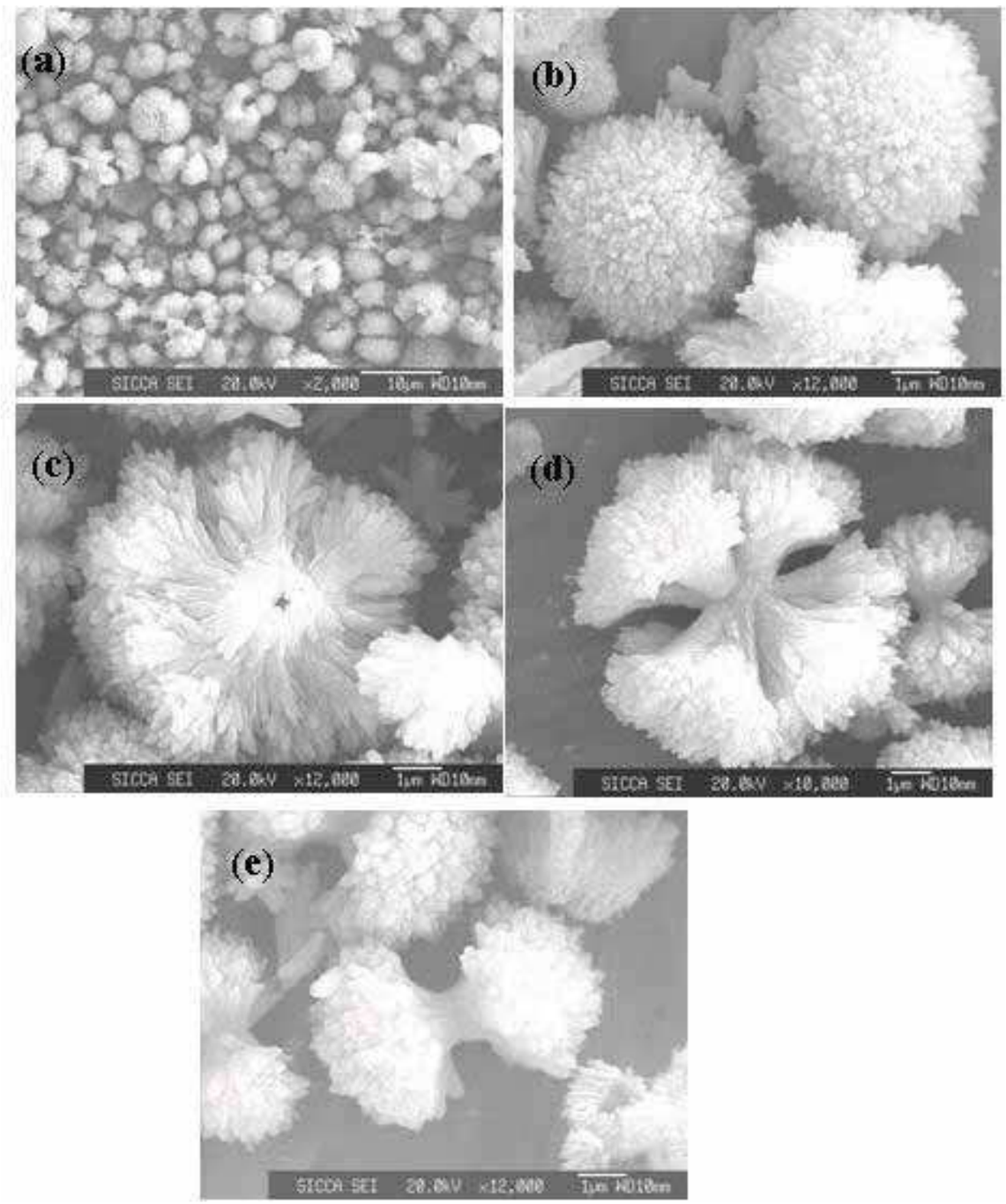


Fig. 11. SEM micrographs of $SrCO_3$ prepared by microwave heating an aqueous solution of $(NH_4)_2CO_3$ and $Sr(NO_3)_2$ at 90 $^oC$ for 5 min. (a) at a low magnification, (b) the top view of a typical flower-like morphology, (c) the bottom view of a typical flower-like morphology, (d) fully assembled flower-like morphology, (e) a typical bundle-like morphology. Reproduced with permission from J. Nanosci. Nanotechnol. **2007**, *7*, 4552. Copyright **2007** *ASP*.

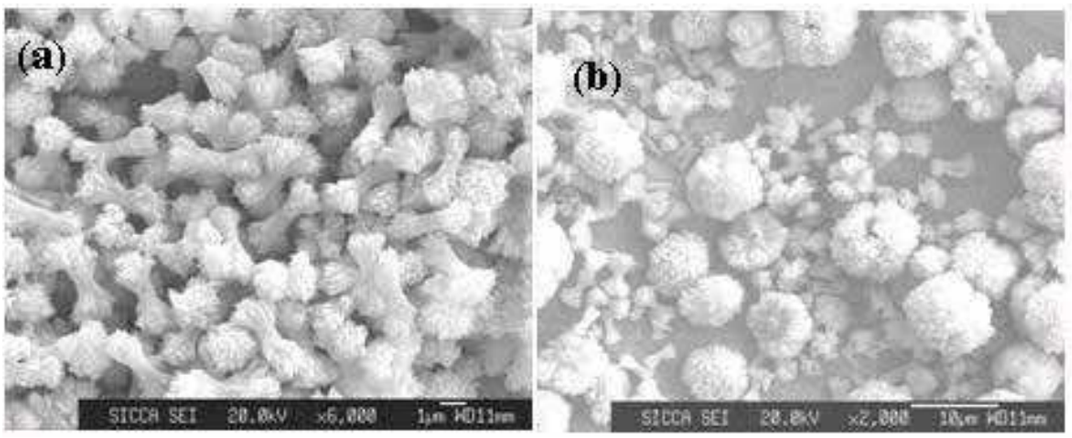


Fig. 12. SEM micrographs of $SrCO_3$ prepared by microwave heating an aqueous solution of $(NH_4)_2CO_3$ and $Sr(NO_3)_2$ at 90 °C. (a) for 30 s, and (b) for 1 min. Reproduced with permission from J. Nanosc. Nanotechn. **2007**, *7*, 4552. Copyright **2007** *ASP*.

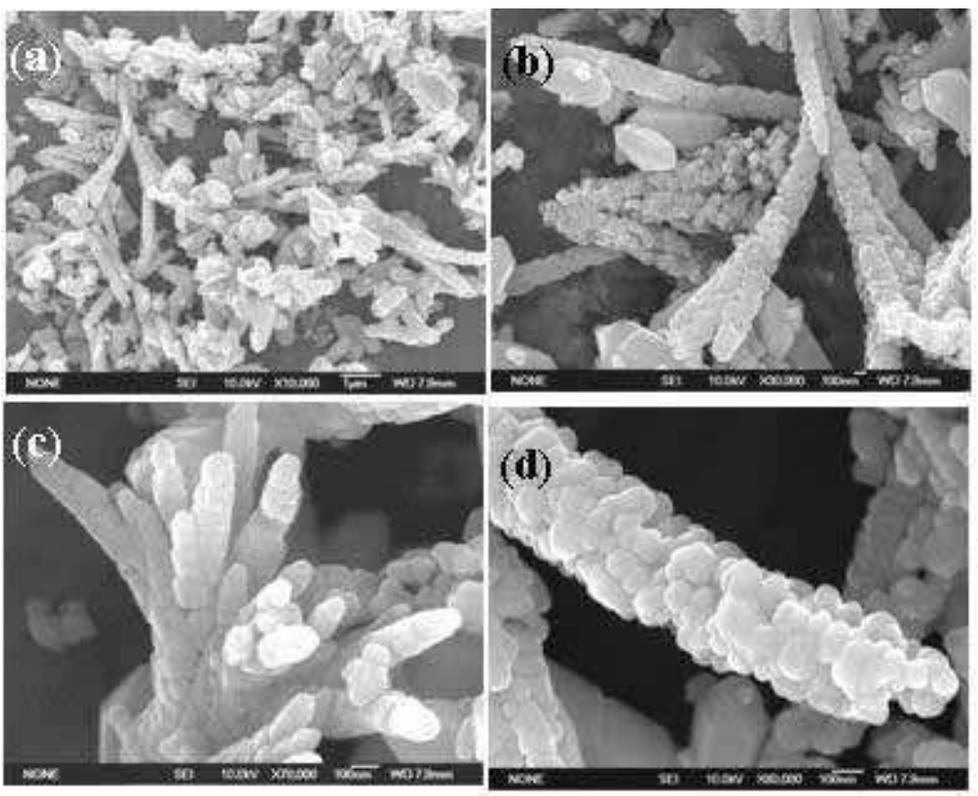


Fig. 13. SEM micrographs of $SrCO_3$ prepared by microwave heating an aqueous solution of $(NH_4)_2CO_3$, $Sr(NO_3)_2$ and EDA at 90 °C for 20 min. (a) at a lower magnification, (b) at a higher magnification, (c) the top view of the branch-like morphology, (d) a typical single branch assembled from nanoparticles. Reproduced with permission from Mater. Lett. **2008**, *62*, 2512. Copyright **2008** *Elsevier*.

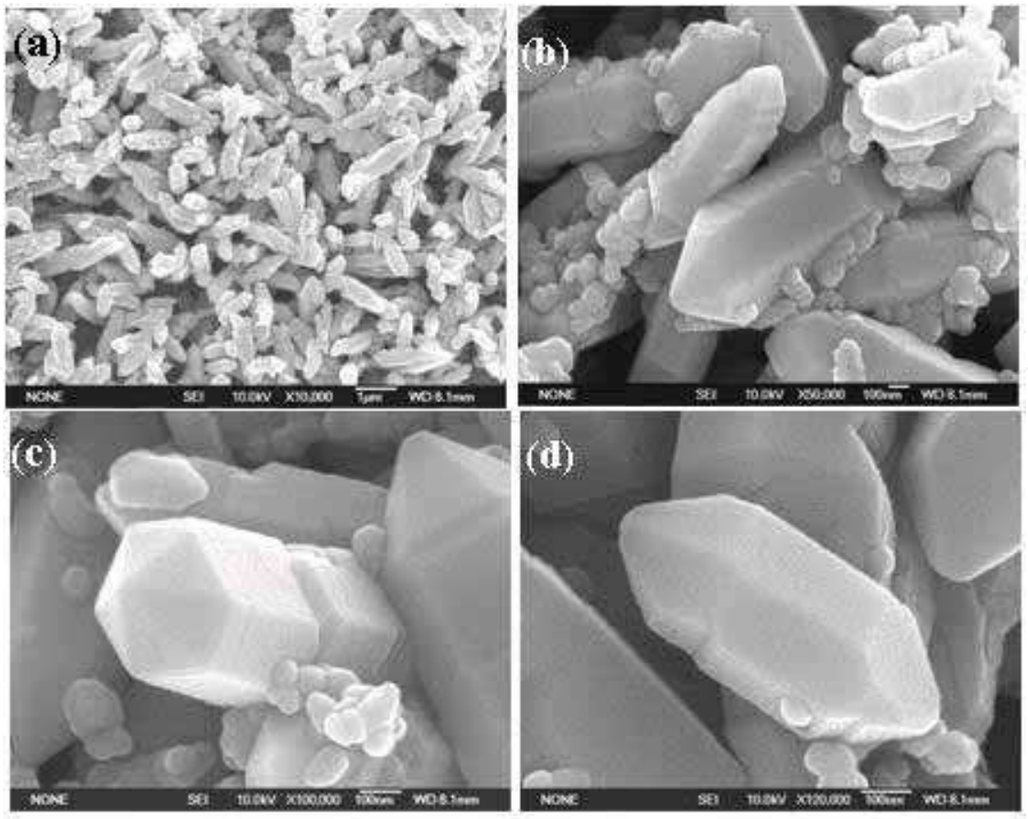


Fig. 14. SEM micrographs of $SrCO_3$ prepared by microwave heating an aqueous solution of $(NH_4)_2CO_3$, $Sr(NO_3)_2$ and ethylenediamine at 90 $^oC$ for 5 min. (a) at a lower magnification, (b) at a higher magnification, (c) the top view of the hexagonal cone, (d) a typical single hexagonal cone. Reproduced with permission from Mater. Lett. **2008**, *62*, 2512. Copyright **2008** *Elsevier*.

Ethylenediamine is a bidentate ligand and has strong coordination ability. In the presence of ethylenediamine, the complex of $Sr(en)_2^{2+}$ formed due to the strong coordination ability of ethylenediamine, then dissolved $Sr^{2+}$ and $CO_3^{2-}$ species would spontaneously form the $SrCO_3$ nuclei at room temperature because of small solubility product of $SrCO_3$ (at 25 $^oC$, $K_{sp}=1.1\times10^{-10}$). Then the $SrCO_3$ nuclei grew to form nanocrystals. The microwave heating leads to a high heating rate and a rapid increase in temperature during the nucleation process, which is important for fast nucleation and growth of crystals. The rapidly changing electric field of the microwave reactor induced the oriented self-assembly of $SrCO_3$ nanocrystals. The self-assembly of nanocrystals depends on the interparticle interactions, crystal size distribution and shape. The microwave heating favored the formation of nanoparticles with a narrow size distribution. Ethylenediamine molecules also acted as the capping ligands that selectively adsorbed onto the surfaces of nanocrystals, leading to the oriented self-assembly of $SrCO_3$ nanocrystals to form branch-like morphology.

Barium chromate ($BaCrO_4$, also called hshemite) is often used as an oxidizing agent, as a catalyst for enhancing vapor-phase oxidation reactions (Economy et al., 1965) and as a highly efficient photocatalyst with a response to visible light irradiation (Yin et al., 2003). $BaCrO_4$ with various morphologies (Ma et al., 2009) such as X-shaped, shuttle, rhombus was produced by using poly(ethylene oxide)-poly(propylene oxide)-poly(ethylene oxide) (P123) as a structure directing agent at room temperature.

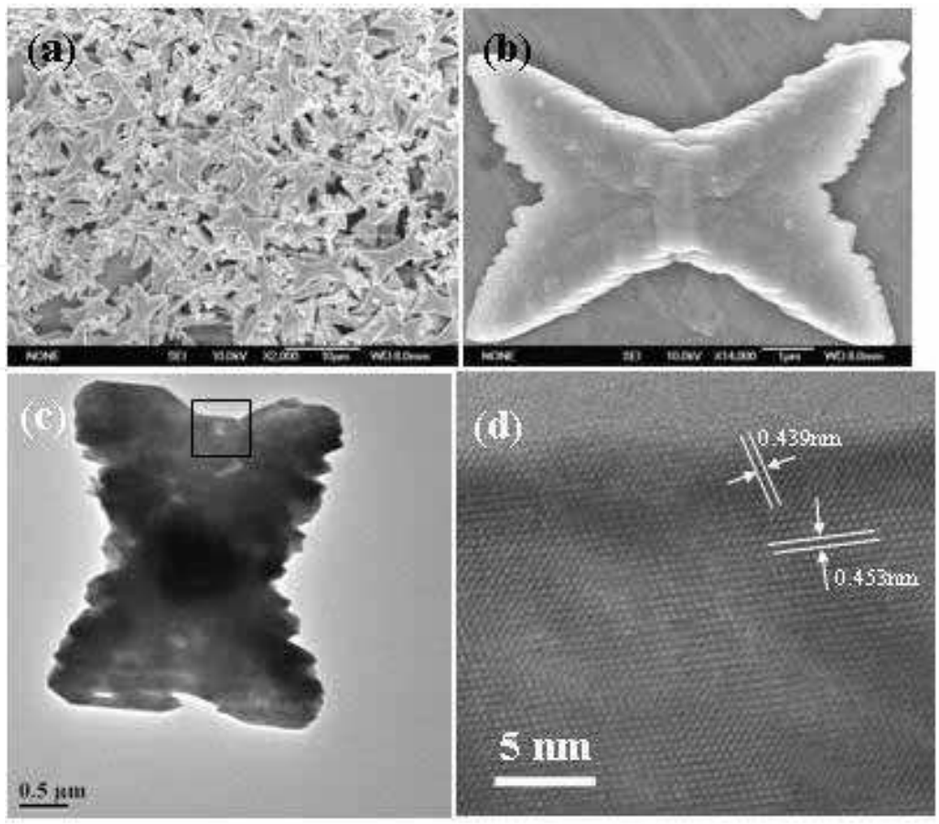


Fig. 15. (a) XRD pattern; (b) and (c) SEM micrographs; and (d) TEM micrograph of the typical $BaCrO_4$ sample. The HRTEM image of the individual X-shaped structure shown in (d) is given in (e). Reproduced with permission from Mater. Res. Bull., **2009**, *44*, 288. Copyright **2009** *Elsevier*.

The typical sample prepared from the solution containing $Ba(NO_3)_2$, $K_2CrO_4$, NaOH and P123 for 12 h. The reflection peaks can be indexed to a single phase of $BaCrO_4$ with an orthorhombic structure (JCPDS 35-0642). The morphology of the product was investigated by SEM, as shown in Fig. 15b and c, indicating that the sample consisted of X-shaped structures (majority) and some flower-like assembly (minority). Fig. 15c shows an individual X-shaped $BaCrO_4$ structure with four branches. Sawtooth-like edge and clear growth steps can be seen from Fig. 15c. The morphology was further investigated by TEM. Fig. 15d shows the typical individual structure. The corresponding SAED pattern of an individual X-shaped $BaCrO_4$ structure indicates the single-crystalline structure of the $BaCrO_4$. Fig. 15e shows the corresponding HR-TEM micrograph of an individual X-shaped $BaCrO_4$ structure. The periodic fringe spacings of ~4.53 and 4.39 Å correspond to the d-spacing of (200) and (011) planes, respectively. This result is in accord with the SAED result.

In our experiment, the sample underwent the ripening process. In order to investigate the effect of time on the morphology of $BaCrO_4$, the samples were fabricated for different times. When the time was only 5 min (Fig. 16a), the shuttle-like morphology with relatively uniform sizes was obtained, indicating rapid nucleation and growth process. Sawtooth-like edge and clear growth steps can be seen from the insets of Fig. 16a. When the time was prolonged to 3 h, the similar morphology was observed (Fig. 16b). The second nucleation

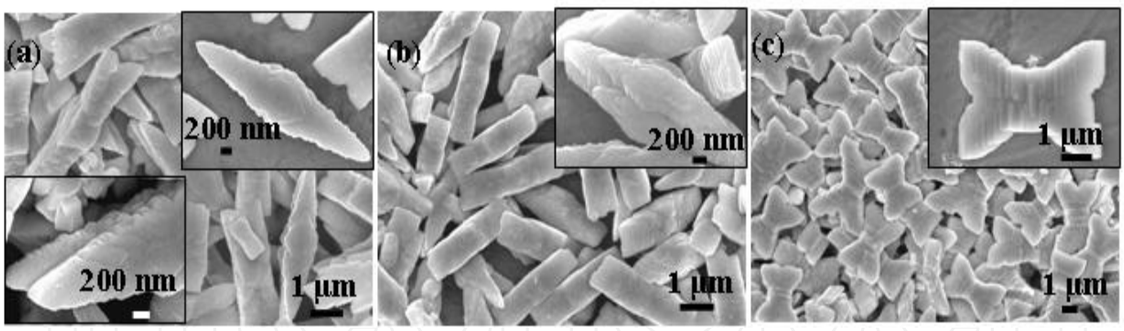


Fig. 16. SEM micrographs of $BaCrO_4$ crystals prepared for different time. (a) 5 min; (b) 3 h; and (c) 6 h. Reproduced with permission from Mater. Res. Bull., **2009**, *44*, 288. Copyright **2009** *Elsevier*.

was observed from the inset of Fig. 16b. When the time was increased to 6 h, the X-shaped structures with four branches with relatively uniform sizes (the lengths were about 2.4 μm) were obtained. From Fig. 16a-c and Fig. 15b, one can clearly see the morphological change process of $BaCrO_4$ with increasing time. The degree of split and the size of X-shaped structures increased with increasing time. The growth mechanism of $BaCrO_4$ may follow the well-known Ostwald ripening process, in which the larger particles grow at the expense of the smaller ones (Sugimoto, 1987).

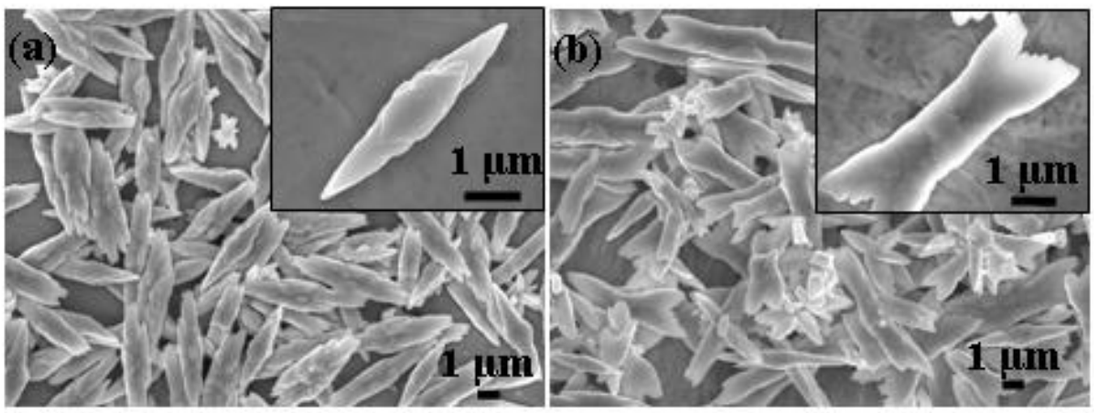


Fig. 17. SEM micrographs of $BaCrO_4$ crystals prepared using different P123 concentration. (a) [P123] = 2.9 g $L^{-1}$ and (b) [P123] = 5.8 g $L^{-1}$. The insets of (a) and (b) show the individual $BaCrO_4$ crystals. Reproduced with permission from Mater. Res. Bull., **2009**, *44*, 288. Copyright **2009** *Elsevier*.

The effect of P123 concentration on the morphology of $BaCrO_4$ was investigated. When the concentration of P123 was increased from 0.58 to 2.9 g $L^{-1}$ and the other conditions were kept the same, the different morphology was obtained (Fig. 17a) compared with Fig. 15b. The shuttle-like morphology was observed. When the concentration of P123 was increased to 5.8 g $L^{-1}$, the size and the morphology were not uniform (Fig. 17b). Therefore, the appropriate concentration of P123 is important for preparing uniform X-shaped morphology of $BaCrO_4$. In the absence of P123, the butterfly-like morphology was obtained (Fig. 18a). In the absence of both P123 and NaOH, the cross-like branches were observed (Fig. 18b). The insets of (a) and (b) show the individual $BaCrO_4$ structures. It is well known that $CrO_4^{2-}$ ions exist in a

basic solution, $Cr_2O_7^{2-}$ ions exist in an acid solution, and $CrO_4^{2-}$ and $Cr_2O_7^{2-}$ can transform to each other in the aqueous solution. So the addition of NaOH favors the synthesis of $BaCrO_4$.

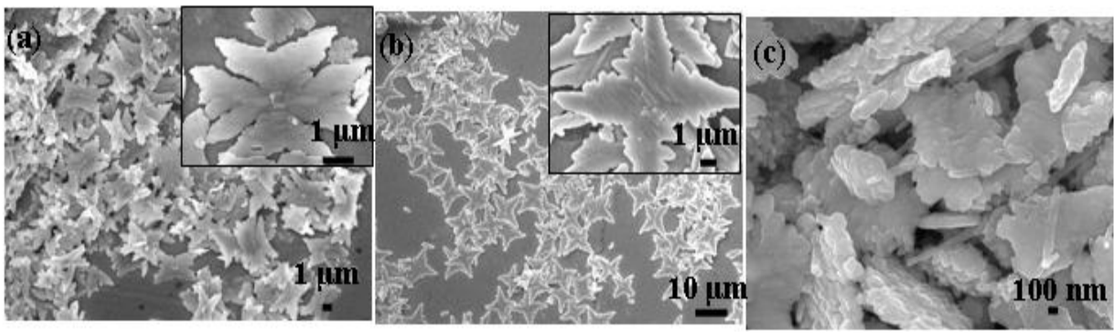


Fig. 18. SEM micrographs of $BaCrO_4$ structures. (a) in the absence of P123; (b) in the absence of P123 and NaOH; (c) 15 mL 0.58 g $L^{-1}$ P123, $Ba(NO_3)_2$ concentration increased from 0.05 to 0.20 mol $L^{-1}$ (0.5 mL), 1 mL 0.50 mol $L^{-1}$ NaOH. Reproduced with permission from Mater. Res. Bull., **2009**, *44*, 288. Copyright **2009** *Elsevier*.

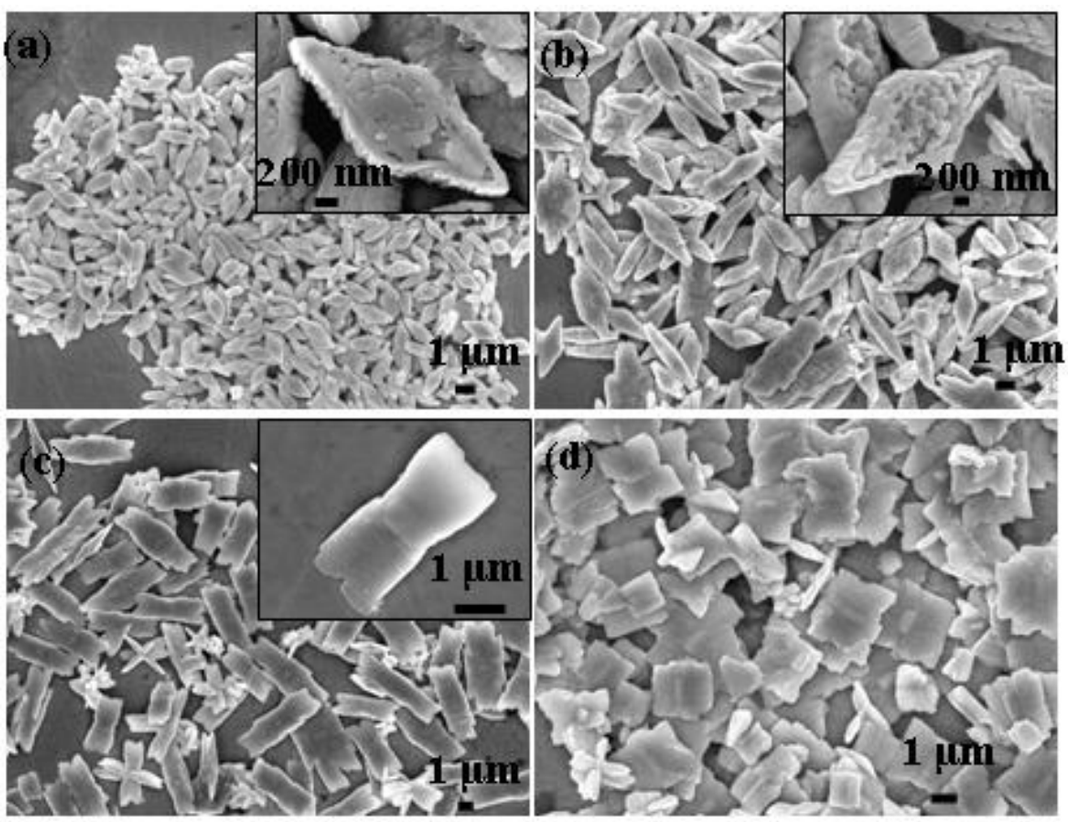


Fig. 19. (a)-(c) SEM micrographs of $BaCrO_4$ crystals prepared in the presence of both P123 and CTAB. (a) [P123] = 0.580 g $L^{-1}$, 6 h; (b) [P123] = 0.580 g $L^{-1}$, 12 h; (c) [P123] = 5.80 g $L^{-1}$, 12 h. (d) SEM micrograph of $BaCrO_4$ crystals prepared in the presence of CTAB. The insets of (a), (b), and (c) show the individual $BaCrO_4$ crystal. Reproduced with permission from Mater. Res. Bull., **2009**, *44*, 288. Copyright **2009** *Elsevier*.

When increasing the concentration of $Ba^{2+}$ from 0.05 mol $L^{-1}$ to 0.20 mol $L^{-1}$, the flakes consisted of particles were observed (Fig. 18c). When the high concentration of $Ba^{2+}$ was used, the nucleation of $BaCrO_4$ was fast and the growth was restricted. So the particles were obtained. These results indicate that the morphology of $BaCrO_4$ is sensitive to the experimental conditions.

The combination effect of P123 and CTAB on the morphology of $BaCrO_4$ was investigated (Fig.19). When both P123 and CTAB were used, the rhombus-like structures consisted of particles were observed and porous structures were seen on the surface. The sizes of rhombus-like structures increased with increasing time. However, when the concentration of P123 was increased from 0.58 to 5.80 mol $L^{-1}$, different morphology was observed (Fig. 19c). When only CTAB was used without P123, the sheet-like morphology was obtained (Fig. 19d).

Various factors including inorganic anions, organic additives and solvents have effects on the morphologies of crystals. The specific adsorption of the additive to particular faces inhibits the growth of these faces by lowering their surface energy, induced the anisotropic

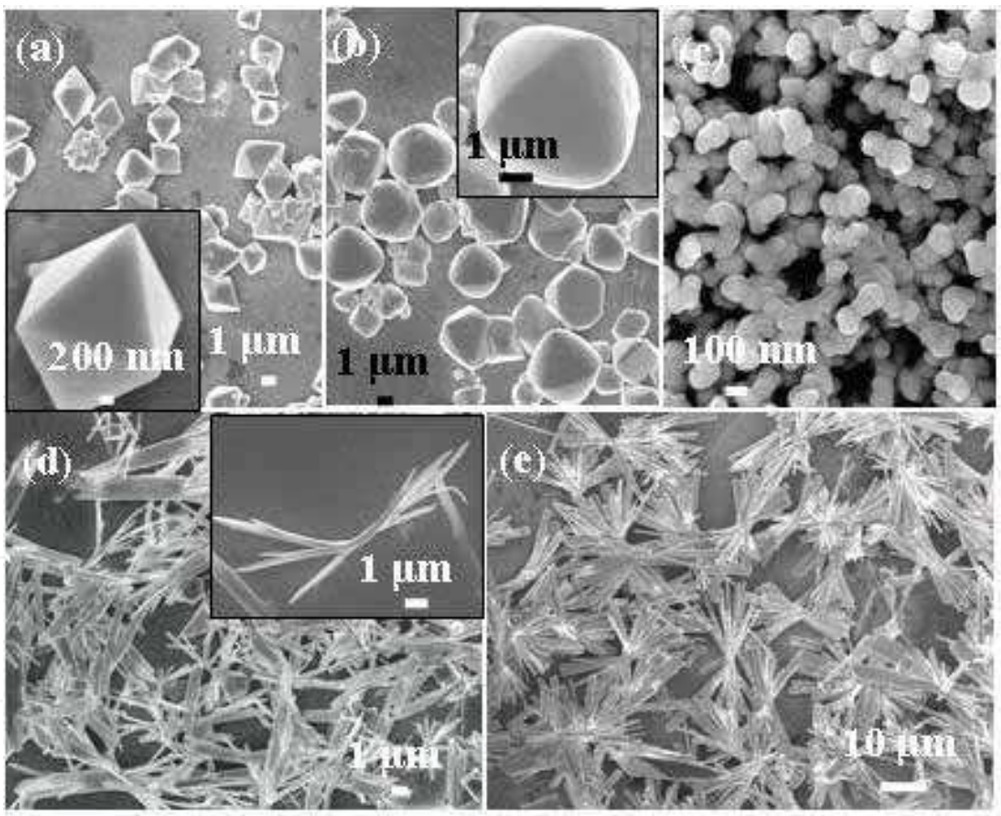


Fig. 20. (a)-(c) SEM micrographs of $BaWO_4$ crystals prepared from the solution of 15 mL P123, 0.5 mL 0.05 mol $L^{-1}$ $Ba(NO_3)_2$, 1 mL 0.50 mol $L^{-1}$ NaOH, and 0.5 mL 0.05 mol $L^{-1}$ $Na_2WO_4$ for 12 h. (a) [P123]= 0.580 g $L^{-1}$; (b) [P123]= 5.80 g $L^{-1}$; (c) in the absence of P123 and NaOH. (d) and (e) SEM micrographs of $Pb_2CrO_5$ crystals prepared from the solution of 15 mL 0.580 g $L^{-1}$ P123, 0.5 mL 0.05 mol $L^{-1}$ $Pb(NO_3)_2$, 1 mL 0.50 mol $L^{-1}$ NaOH, and 0.5 mL 0.05 mol $L^{-1}$ $Na_2CrO_4$.: (d) 6 h; (e) 12 h. The insets of (a), (b) and (d) show the individual crystal. Reproduced with permission from Mater. Res. Bull., **2009**, *44*, 288. Copyright **2009** *Elsevier*.

growth of the crystals, and influenced the crystal morphology. Due to the electrostatic interaction with $Ba^{2+}$ ions, the negatively charged of polymer polar groups acted as active sites for the nucleation of $BaCrO_4$. Yu et al. (2003) reported that some faces of the $BaCrO_4$ crystal could adsorb negatively charged groups such as $-PO_3H_2$, –COOH of polymer by electrostatic attraction and block these faces from further growth. Some interesting morphologies prepared using both polymer and surfactant as crystallization templates were reported (Shi et al., 2003; Wei et al., 2004a,b).

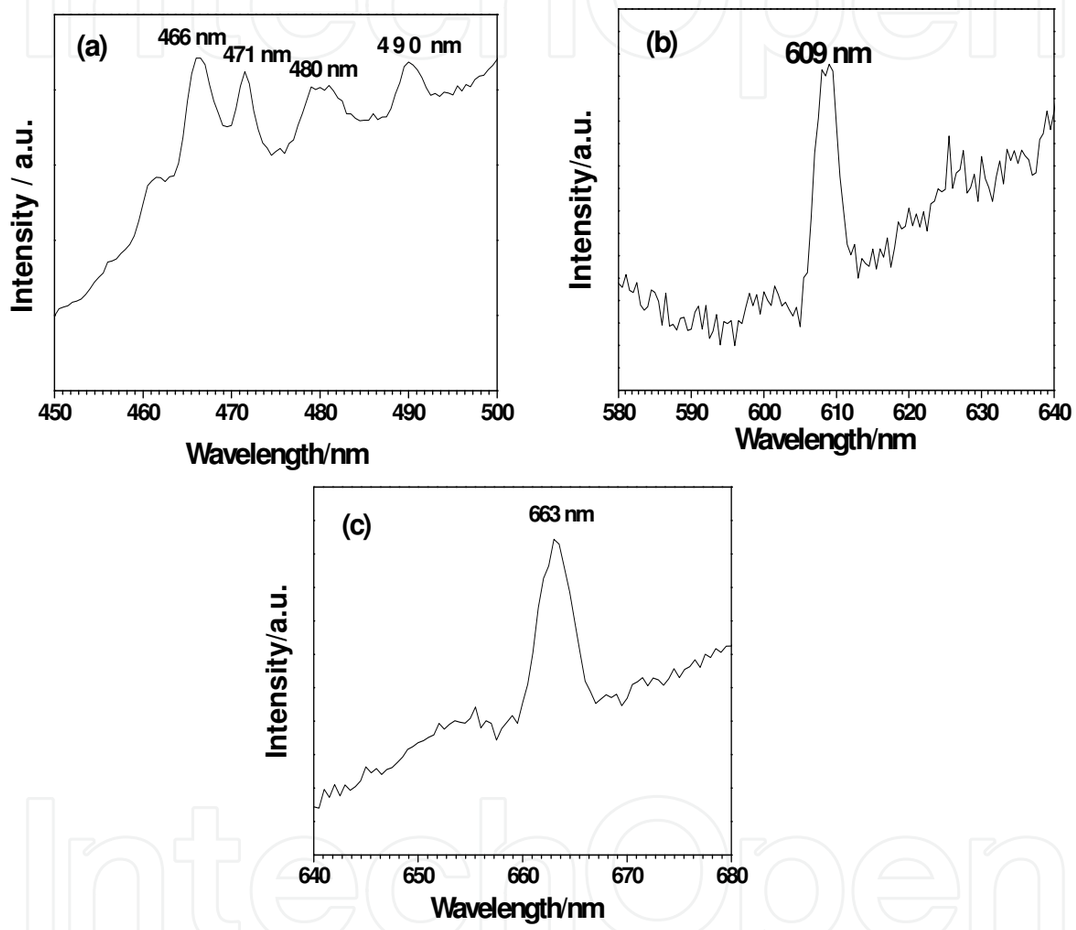


Fig. 21. PL spectra of the $BaCrO_4$ sample as shown in Fig. 15: (a) $\lambda_{ex}$ = 276 nm; (b) $\lambda_{ex}$ = 454 nm; (c) $\lambda_{ex}$ = 488 nm. Reproduced with permission from Mater. Res. Bull., **2009**, *44*, 288. Copyright **2009** *Elsevier*.

$BaWO_4$ and $Pb_2CrO_5$ were slao fabricated using this synthetic route, and the corresponding results were displayed in Fig.6. The $BaWO_4$ sample consisted of octahedral crystals (Fig. 20a). The XRD pattern shows that the sample consisted of a single phase of crystalline tetragonal sheelite type $BaWO_4$ (JCPDS 43-0646). When the concentration of P123 was increased from 0.580 to 5.80 mol $L^{-1}$, the polyhedrons were observed (Fig. 20b). In the absence of P123 and NaOH, $BaWO_4$ particles were obtained (Fig. 20c), which is different

from the morphologies in Fig. 20a and b. Fig. 20d shows the SEM micrograph of the $Pb_2CrO_5$ sample synthesized for 6 h, the long flakes with the split at two ends were observed. The inset of Fig. 6d displays the detailed structure. When the time was increased to 12 h, the bundles of nanoflakes were obtained (Fig. 20e). The XRD pattern shows that the sample consisted of a single phase of crystalline monoclinic $Pb_2CrO_5$ (JCPDS 29-0768).

Recently, the diverse luminescent spectra of $BaCrO_4$ were obtained when $BaCrO_4$ (Yan et al., 2006) was excited by 276, 454 and 488 nm, respectively. The PL spectra of our $BaCrO_4$ sample were obtained using the same excitation wavelengths. When excited at 276 nm, four weak emission band peaks were observed at 466, 471, 480, and 490 nm (Fig.21a). The emission band peak was not observed in the range of 300-450 nm. When excited at 454 and 488 nm, the $BaCrO_4$ sample had the strong emission band peak at 609 and 663 nm (Fig. 21b and c), respectively. Using the same excitation wavelength, Yan et al. (2006) observed the broad emission band peaks appeared at 607 and 640 nm, respectively. This phenomenon indicated that the $BaCrO_4$ sample had the diverse luminescent properties and potential application in electronic devices. Blasse (1980) proposed that the isoelectronic system $CrO_4^{2-}$ was nonluminescent because of rapid radiationless deactivation. The metastable triplet state of the chromate ion may have an effect on the luminescent properties of $BaCrO_4$ (Dalhoeven et al., 1980; Miller & Tinti,1986; Speket al., 1996). The intrinsic mechanism still needs to be investigated because of few reports about luminescent properties of $BaCrO_4$ sample.

## 4. Morphology, structure, and function biomineral synthesis of other nanomaterials

Biomineral synthesis includes morphology, structure, and function biomineral synthesis. It is well known that the structure determines property and the morphology is the external display of structure. In chemistry, biomimetic synthesis is a man-made chemical synthesis inspired by biochemical processes. Here, we intend to review recent progress in biomineral synthesis of other nanomaterials in this section.

Fig. 22. The non-wetting leg of a water strider. **a,** Typical side view of a maximal-depth dimple (4.38±0.02 mm) just before the leg pierces the water surface. Inset, water droplet on a leg; this makes a contact angle of 167.6±4.4°. **b, c,** Scanning electron microscope images of a leg showing numerous oriented spindly microsetae (**b**) and the fine nanoscale grooved structures on a seta (**c**). Scale bars: **b,** 20 μm; **c,** 200 nm. Reproduced with permission from Nature, **2004**, *432*, 36. Copyright **2004** *Nature Publishing Group*.

Since the discovery of carbon nanotubes in 1991 (Iijima, 1991), carbon and carbon-based nanocomposites have been receiving more attention due to its unique properties such as

mechanical properties, high thermal stability, electrical properties, high-temperature and high-pressure stability and resists attacks from acids, bases, and solvents, and promising potential applications in electronic conductors (White & Todorov, 1998), microelectrode (Teo et al., 2005), field emission transistors (Keren et al., 2003), hydrogen storage (Lin, 2000). carbon nanotubes are a excellent candidate in biomineral synthesis field.

Many biological surfaces in both the plant and animal kingdom possess unusual structural features at the micro- and nanometre-scale that control their interaction with water and hence wettability. Some paints and roof tiles have been engineered to be self-cleaning by copying the mechanism from the Nelumbo lotus. Jiang et al. reveal the mechanism of standing effortlessly and moving quickly on water of water striders in 2004 (Gao & Jiang, 2004), which has unique hierarchical micro- and nanostructuring on the leg's surface (Fig. 22). This discovery favors in the design of miniature aquatic devices and non-wetting materials. They also discover the micro- and nanoscale hierarchical structures on the surface of a lotus leaf (branch-like nanostructures on top of the micropapillae), which can induce super-hydrophobic surfaces with large contact angle and small sliding angle (Fig. 23a,b) (Zhai et al., 2002) and the micro- and nanostructures of a rice leaf, which are arranged in

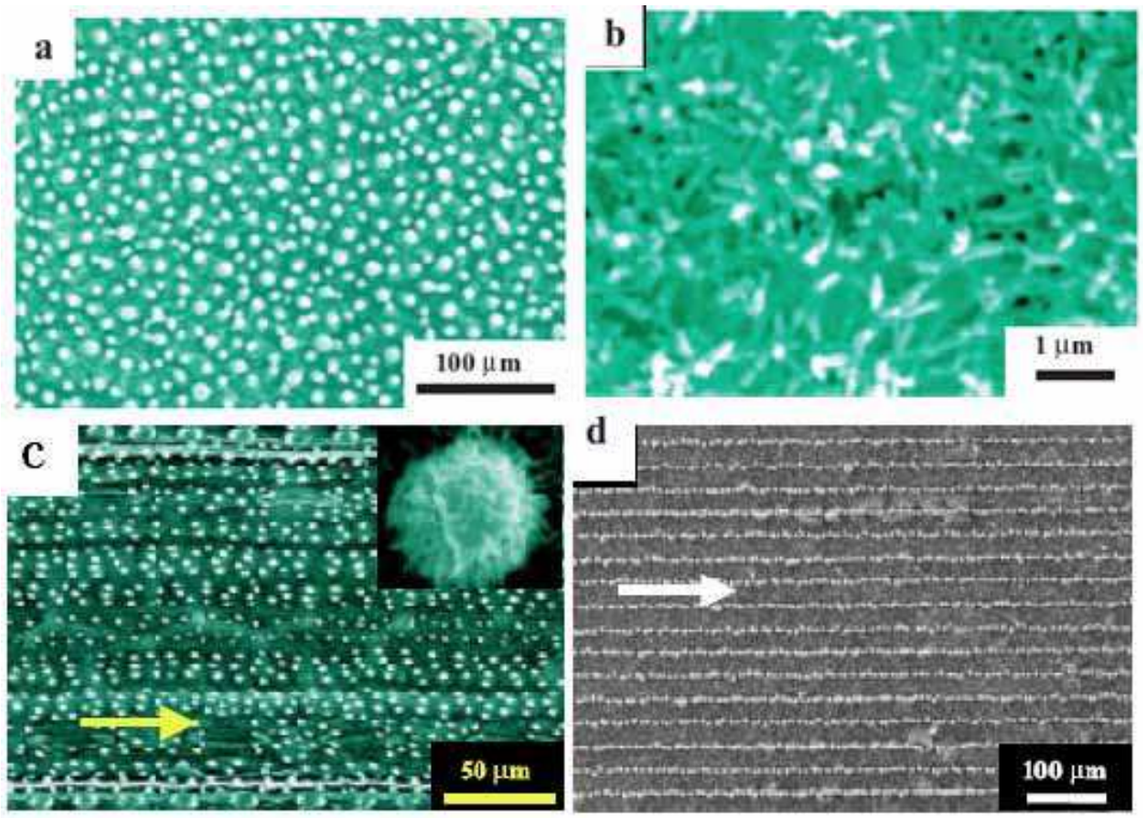


Fig. 23. a)Large-area SEM image of the surface of a lotus leaf (*Nelumbo nucifera*). Every epidermal cell forms a papilla and has a dense layer of epicuticular waxes superimposed on it. b) SEM image of the lower surface of the lotus leaf. c) Large-area SEM image of the surface of a rice leaf (*Oryza sativa*) with different magnifications. d) SEM image of the top view of a rice-like ACNT film. Reproduced with permission from Physics, **2002**, *31*, 483 and Adv. Mater., **2002**, *14*, 1857. Copyright **2002** *Elsevier and VCH*.

one-dimensional order parallel to the leaf edge with sliding angle 3-5° and randomly in the other directions with sliding angle 9-15° (Fig. 23c). Based on the finding, they biomineral synthesized the rice-like aligned carbon nanotube films with the similar micro- and nanostructures with super-hydrophobic nanochannels (Fig. 23d) (Feng et al., 2002). Aligned structure of carbon nanotube films with fairly uniform length of (3 μm) and external diameter (60 nm) and super-amphiphobic properties was biomineral synthesized by high temperature pyrolysis method using phthalocyanine complexes as raw materials (Li et al., 2001). The experimental results show that the untreated aligned carbon nanotube films are super-hydrophobic and super-lipophilic, fluoride membrane surface modification of carbon nanotubes are both hydrophobic and lipophobic properties, indicating that the presence of nanostructure led to the super-amphiphobic surface. Moreover, they designed artificial fibres that mimic the structural features of silk and exhibit its directional water-collecting ability, inspired by the finding that the water-collecting ability of the capture silk of the cribellate spider *Uloborus walckenaerius* is the result of a unique fibre structure that forms after wetting, with the 'wet-rebuilt' fibres characterized by periodic spindle-knots made of random nanofibrils and separated by joints made of aligned nanofibrils (Zheng et al., 2010). It is well known that the ability of gecko lizards to adhere to a vertical solid surface is due to their remarkable feet with aligned microscopic elastic hairs. Qu et al. (2008) biomineral

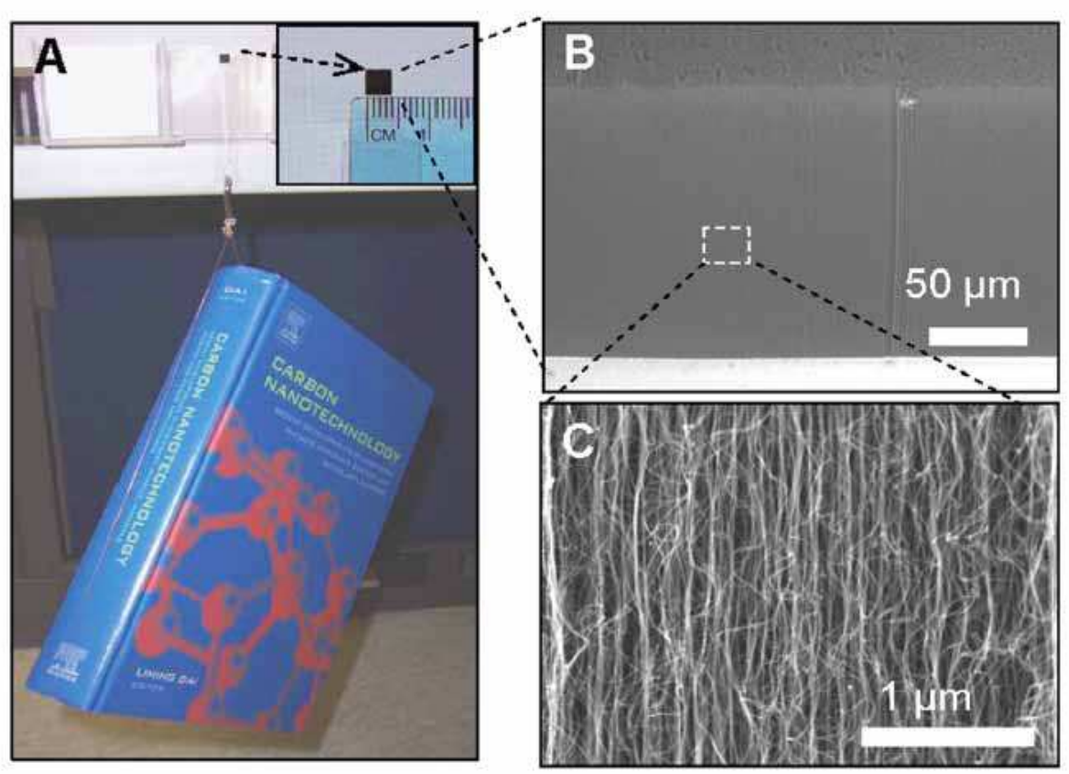


Fig. 24. (A) A book of 1480 g in weight suspended from a glass surface with use of VA-MWNTs supported on a silicon wafer. The top right squared area shows the VA-MWNT array film, 4 mm by 4 mm. (B and C) SEM images of the VA-MWNT film under different magnifications. Reproduced with permission from *Science*. **2008**, *322*, 238. Copyright **2008** *AAAS*.

synthesized the gecko-foot-mimetic dry adhesives with macroscopic adhesive forces of ~100 newtons per square centimeter using carbon nanotube arrays by simulating the walking of a living gecko (Fig. 24).

Bioinspired synthesis and self-assembly of advanced inorganic materials is fascinating field. Yu and co-workers used biomimetic synthesis method, in which the mineralization of inorganic materials was carried out in a glass bottle, which was put into a closed dessicator at room temperature, similar to that described by Addadi and co-workers (1996).

Yu et al (2005). reported the biomimetic synthesis of helices alignment achiral $BaCO_3$ nanocrystals in the presence of double hydrophilic block copolymers by a racemic polymer controlled biomineralization processes through selective adsorption on the (110) face of nanocrystals (Fig. 25). The results show that the spontaneous formation of spiral structure can be fabricated by directed tectonic assembly of inorganic particles and a new mechanism of the formation of spiral structure was proposed, that due to non-homogeneous polymer adsorption, making new modes of spontaneous symmetry breaking on the mesoscale, generating chiral contributions in the mutual interaction potentials of the building blocks. Moreover, facile biomimetic method is reported for the synthesis of novel $BaCO_3$ nanofibres with double-stranded and cylindrical helical morphologies (Zhu et al., 2009) *via* a phosphonated block co-polymer-controlled mineralization process.

Well-defined concaved cuboctahedral superstructures of copper sulfide (Wu et al., 2006) were large scale synthesized by a solvothermal reaction in ethylene glycol (Fig. 26). Each caved cuboctahedron is apparently "caved" with 14 highly symmetric cavities and is constructed by four identical hexagonal flakes while sharing the 24 edges in a dymaxion way. The results demonstrate that the branching growth process in solution can be precisely manipulated for the controlled growth of amazingly complex crystalline structures with high geometrical symmetry, which is not reflected in the primary crystal symmetry. This complex superstructure is similar to the image by M. C. Escher (1948).

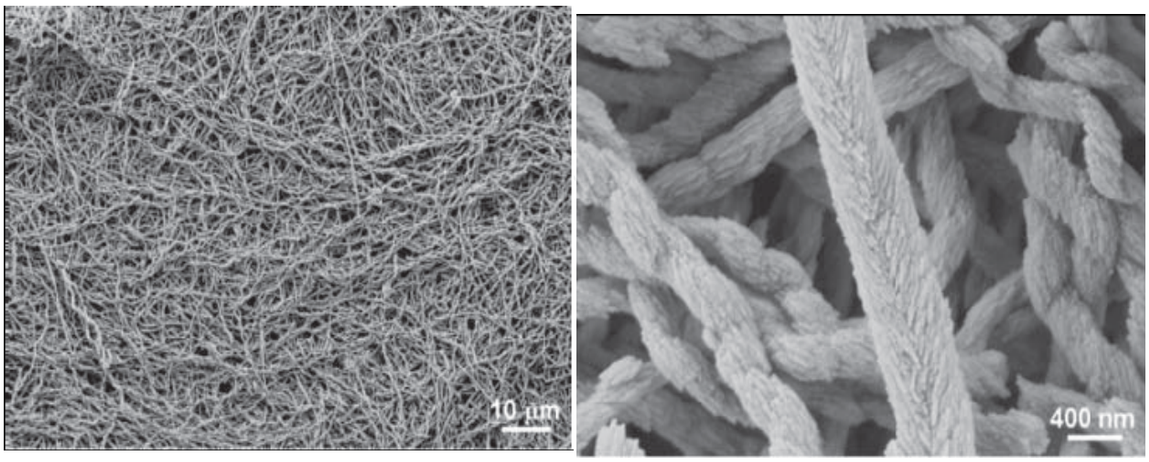


Fig. 25. Helical nanoparticle superstructures. a, The helical fi bres formed at room temperature with PEG-b-DHPOBAEE, 1 gL-1, starting pH=4, [$BaCl_2$] = 10 mM. **b**, Detailed surface structure. Reproduced with permission from *Nature Materials* **2005**, *5*, 51. Copyright **2005** *Nature Publishing Group.*

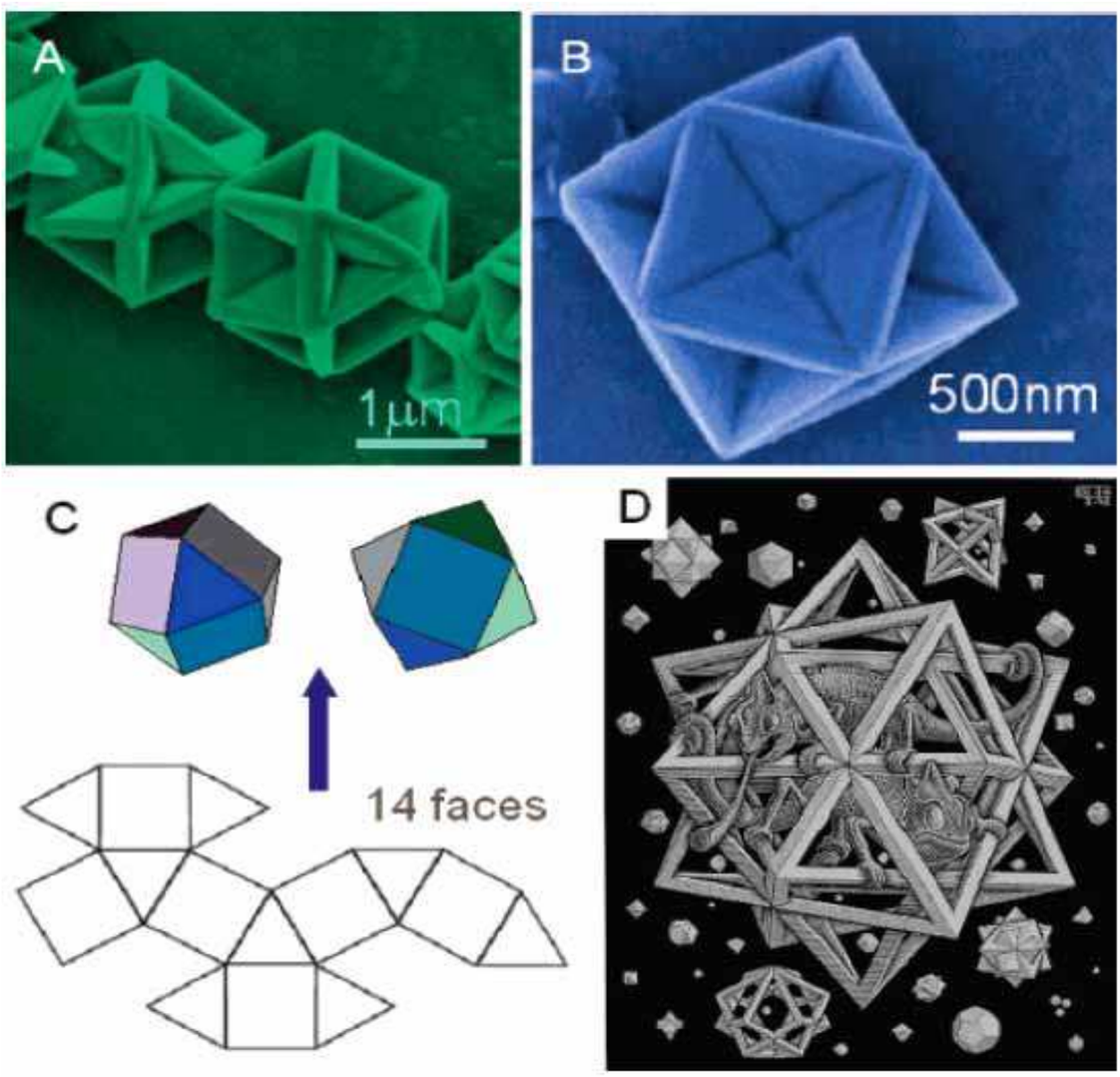


Fig. 26. (A and B) SEM images of the typical caved cuboctahedral crystals, synthesized by the solvothermal process at 140 °C for 24 h. (C) Schematic illustration of a cuboctahedron with 14 faces (six squares and eight triangles), composing the structure by sharing the identical 24 edges in a dymaxion way. (D) Cuboctahedron appearing as one of the polyhedral "stars" in M. C. Escher's 1948 wood engraving *Stars*. Reproduced with permission from Chem. Mater. **2006**, *18*, 3599. Copyright **2006** *ACS*.

The unique necklace-like Cu@cross-linked poly-(vinyl alcohol) (PVA) microcables (Zhan et al., 2008) that have strict wire-bead forms were biomimetic synthesized using a mixture of CuCl and $CuCl_2 \cdot 2H_2O$ by hydrothermal method at lower pH values (Fig. 27). One-dimensional magnetic Ni-Co alloy microwires (Hu & Yu, 2008) with different microstructures and differently shaped building blocks including spherical particles, multilayer stacked alloy plates, and alloy flowers, have been synthesized by an external magnetic field-assisted solvothermal reaction of mixtures of cobalt(II) chloride and nickel(II) chloride in 1, 2-propanediol with different NaOH concentrations (Fig. 28).

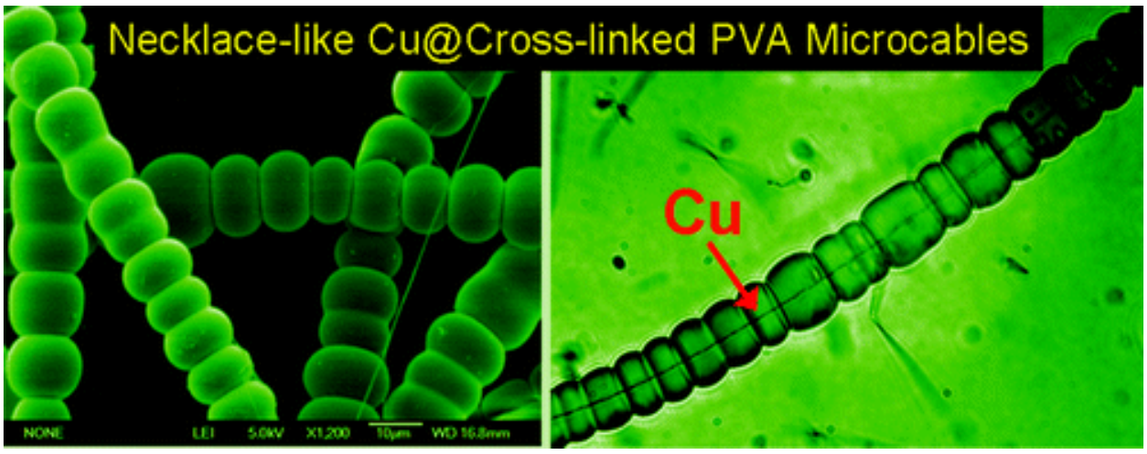


Fig. 27. SEM images of the necklace-like microcables with different magnifications. Reproduced with permission from J. Am. Chem. Soc. **2008**, *130*, 5650. Copyright **2008** *ACS*.

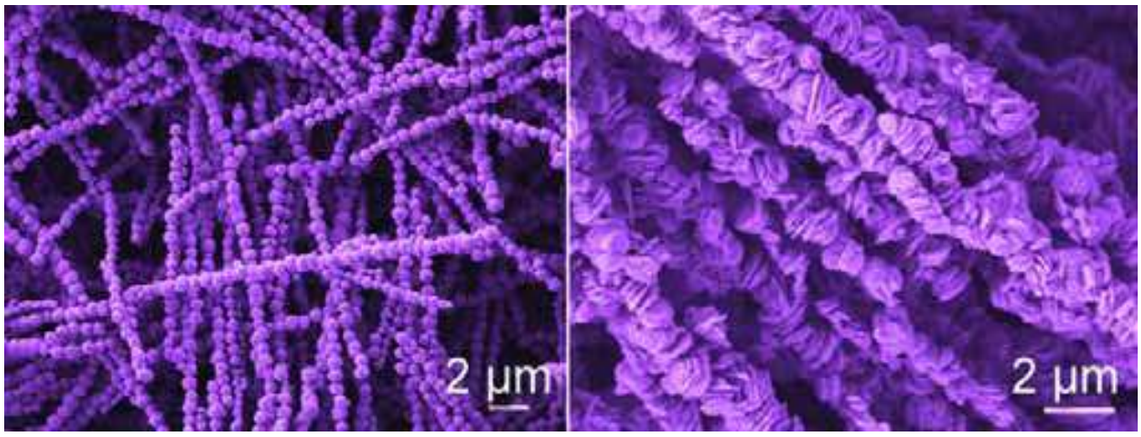


Fig. 28. SEM images of the one-dimensional assembly of $Ni_xCo_{1-x}$ alloy microparticles. Reproduced with permission from Nano Research **2008**, *1*, 303. Copyright **2008** *springer*.

The calcite pancakes with controlled surface structures (Chen et al., 2005) was fabricated by double-hydrophilic block copolymer-directed self-assembly using the macrocycle-coupled block copolymer,poly(ethylene glycol)-b-poly (1,4,7,10,13,16-hexaazacyclooctadecan ethylene imine), macrocycle (PEG-B-hexacyclen) as a crystal modifier (Fig. 29a). Highly monodisperse $CaCO_3$ (vaterite) microspheres (Guo et al., 2006) were prepared by a slow gas-liquid diffusion reaction with an artificial peptide-type block copolymer, PEG(110)-b-pGlu(6), as a crystal-growth modifier in a mixture of solvents by using a suitable volume ratio of N,N-dimethylformamide/nonionic water and by taking advantage of the synergistic effects of the block copolymer and the solvent mixture (Fig. 29b,c). The results demonstrate that the solvent mixture plays a key role in controlling the growth, polymorphism, and shape of the $CaCO_3$ mineral. Polymorph discrimination of $CaCO_3$ mineral in an ethanol/water solution: Formation of complex vaterite superstructures and aragonite rods (Fig. 29d-f) (Chen et al., 2006).

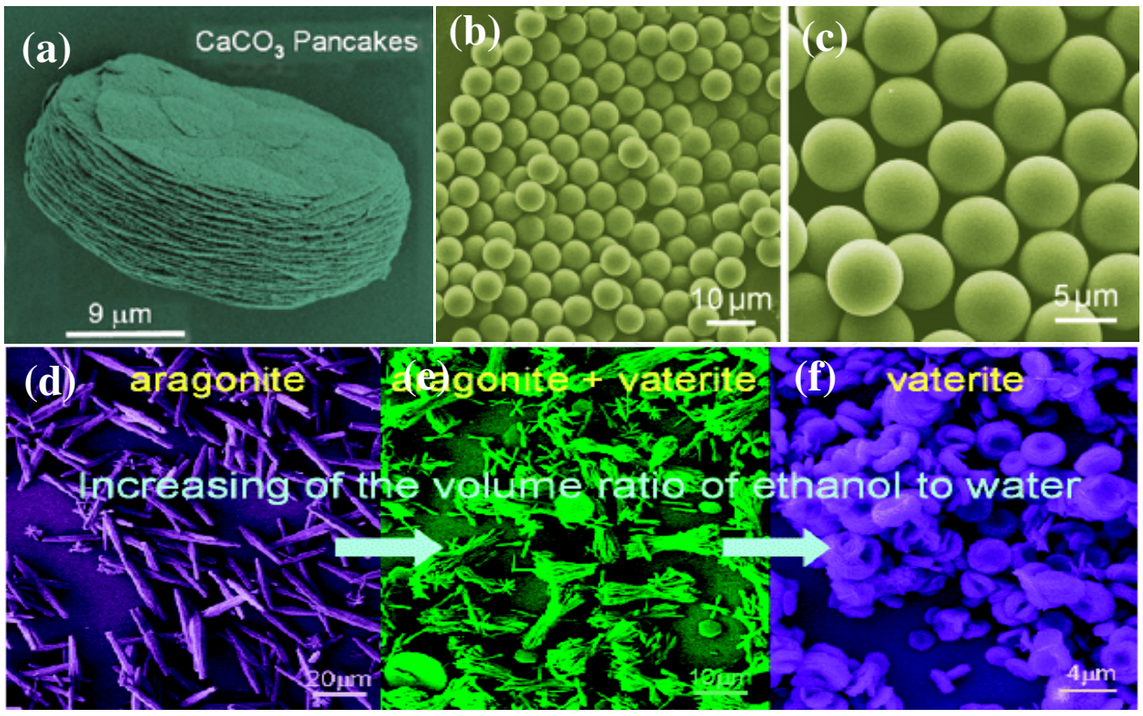


Fig. 29. SEM images of the $CaCO_3$: (a) calcite pancakes; (b,c) monodisperse $CaCO_3$ (vaterite) microspheres; (d-f) vaterite superstructures and aragonite rods. Reproduced with permission from Adv. Mater. **2005**, *17*, 1461, Angew. Chem. Int. Ed. **2006**, *45*, 3977, and Chem. Mater. **2006**, 18, 115. Copyright **2010** *ACS* and *VCH*.

## 5. Conclusion

In recent years, rapid progress has been made in the research of biomineralization and biomimetic synthesis. The effect research of bimolecular on the structure of biomaterials has great scientific significance and widely applications. However, the present research was still at the initial stage. In future, the follow problems should be explored. For example, the relationship of properties and microstructure in biominerals; the intrinsic mechanism of biomineralization; the experimental examples for better understanding of the molecular recognition mechanism; how to simulate the biomineralization and realize biomimetic synthesis?

## 6. Acknowledgments

Financial support from the National Natural Science Foundation of China (31070511) China Postdoctoral Science Special Foundation (20100359), and Major State Basic Research Development Program of China (973 Program) (No.2010CB732204) is gratefully acknowledged.

## 7. References

Banfield, J. F.; Welch, S. A.; Zhang, H. Z.; Ebert, T. T. & Penn, R. L. (2000). *Science* 289,751-54.

Bastow, T. J. (2002). *Chem. Phys. Lett.* 354, 156.
Blasse, G. (1980). *Struct. Bonding*, 42, 1.
Bohner, M. (2004). New hydraulic cements based on a-tricalcium phosphate-calcium sulfate dihydrate mixtures. *Biomaterials*, 25, 741-9.
Boskey, A. L.; Young, M. F.; Kilts, T. &Verdelis, K. (2005). Variation in mineral properties in normal and mutant bones and teeth. *Cells Tissues Organs*, 181, 144-53.
Cameron, H. U.; Macnab, I. & Pilliar, R. M. (1977). Evaluation of a biodegradable ceramic. *J Biomed. Mater. Res.*, 11, 179-86.
Chen, S. F.; Yu, S. H.; Jiang, J.; Li, F. Q. & Liu, Y. K. (2006). Polymorph discrimination of $CaCO_3$ mineral in an ethanol/water solution: Formation of complex vaterite superstructures and aragonite rods. *Chem. Mater., 18*, 115-122.
Chen, S. F.; Yu, S. H.; Wang, T. X.; Jiang, J.; Cölfen, H.; Hu, B. & Yu, B. (2005). Polymer directed formation of unusual $CaCO_3$ pancakes with controlled surface structures. *Adv. Mater., 17*, 1461-1465.
Cheng, X. K.; He, Q. J.; Li, J. Q.; Huang, Z. L. & Chi, R. A. (2009). Control of pore size of the bubble-template porous carbonated hydroxyapatite microsphere by the adjustable pressure. *Crystal Growth & Design*, 9, 2770-5.
Chi, C. W. (2010). US7687098.
Chow, L. C. & Sun, L. M. (2010). US7670579.
Cortes, D. A.; Medina, A.; Escobedo, J. C.; Escobedo, S. & Lopez, M. A. (2004). Effect of wollastonite ceramics and bioactive glass on the formation of a bonelike apatite layer on a cobalt base alloy. *J Biomed. Mater. Res.* A 70A, 341-6.
Cotton, F. A.; Wilkinson, G.; Murillo, C. A. & Bochmann, M. (1999). *Adv. Inorganic Chem. 6th ed.*; Wiley: New York.
Cui, X. J.; Yu, S. H.; Li, L. L.; Biao, L.; Li, H. B.; Mo, M. S. & Liu, X. M. (2004). *Chem. Eur. J*, 10, 218-23.
Dadyburjor, D. B. & Ruckenstein, E. (1977). *J Cryst. Growth*, 40, 279.
Dalhoeven, G. A. M. & Blasse, G. (1980). *Chem. Phys. Lett.*, 76, 27-29.
Ding, S. J. (2009). US2009198345.
Dorozhkin, S. V. (2007). Calcium orthophosphates. *J Mater. Sci.*, 42, 1061-95.
Economy, J.; Meloon Jr., D. T. & Ostrozynski, R. L. (1965). *J Catal.* 4, 446.
Erdemoğlu, M. & Canbazoğlu, M. (1998). *Hydrometallurgy* 49, 135.
Escher, M. C. *Stars* wood engraving, 1948; http://www.mcescher.com/Gallery/back-bmp/LW359.jpg.
Feng, L.; Li, S. H.; Li, Y. S.; Li, H. J.; Zhang, L. J.; Zhai, J.; Song, Y. L.; Liu,B. Q.; Jiang, L.; & Zhu. D. B. (2002). Super-hydrophobic Surfaces: From Natural to Artificial. *Adv. Mater.*, 14, 1857
Fujii, S.; Okada, M.; Sawa, H.; Furuzono, T. & Nakamura, Y. (2009). Hydroxyapatite nanoparticles as particulate emulsifier: fabrication of hydroxyapatite-coated biodegradable microspheres. *Langmuir* 25, 9759-66.
Furuzono, T.; Kisida, A.; Tanaka, J. & Matsuda, A. (2009). US7473731.
Gao, F.; Lu, Q. Y.; Xie, S. H. & Zhao, D. Y. (2002). *Adv. Mater.* 14,1537-40.
Gao, X. F. & Jiang, L. (2004). Striking water repellence by water striders' legs. *Nature*, 432,36
Garcia-Sanz, F. J.; Mayor, M. B.; Arias, J. L.; Pou, J.; Leon, B. & Perez-Amor, M. (1997). Hydroxyapatite coatings: a comparative study between plasma-spray and pulsed laser deposition techniques. *J Mater. Sci. Mater. Med.*, 8, 861-5.

Getter, L.; Bhaskar, S. N.; Cutright, D. E.; Perez, B.; Brady, J. M.; Driskell, T. D. & O'Hara, M. J. (1972). Three biodegradable calcium phosphate slurry implants in bone. *J Oral. Surg.*, 30, 263-8.

Gindl, W. & Keckes, J. (2004). Tensile properties of cellulose acetate butyrate composites reinforced with bacterial cellulose. *Comp. Sci. Techn.*, 64, 2407-13.

Godber, J. & Leite, L. (2009). US7468172.

Griffiths, J. (1985). *Ind. Miner.* 218, 21.

Groot, D. & Mitchell, J. C. (1981). Oro-pharyngeal mucosal reaction to fenoterol. *Contact Dermatitis*, 7, 48.

Gross, K. A; Berndt, C. C. & Iacono, V. J. (1998). Variability of hydroxyapatite-coated dental implants. *Int. J Oral. Maxillofac Implants*, 13, 601-610.

Gross, K. A.; Ray, N. & Rokkum, M. (2002). The contribution of coating microstructure to degradation and particle release in hydroxyapatite coated prostheses. *J, Biomed, Mater, Res.*, 63, 106-14.

Guo, X. H.; Yu, S. H. & Cai, G. B. (2006). A New controlled crystallization approach in a mixed solution using an artificial peptide type block copolymer as a crystal modifier: highly monodisperse $CaCO_3$ microspheres and morphology control. *Angew. Chem. Int. Ed., 45*, 3977-3981.

Gutmann, B. & Chalup, A. (2000). *Am. Ceram. Soc. Bull.* 79, 63.

Hing, K. A. (2004). Bone repair in the twenty-first century: biology, chemistry or engineering. *Philos. Trans. R. Soc. A* 362, 2821-50.

Hu,M. J.; Lin, B. & Yu, S. H. (2008). Magnetic-Field Induced Solvothermal Synthesis of Uniform One-Dimensional Assembly of $Ni_xCo_{1-x}$ Alloy Microparticles. *Nano Research,1*, 303-312.

Iguchi, M.; Yamanaka, S. & Budhiono, A. (2000). Bacterial cellulose-a masterpiece of nature's arts. *J Mater. Sci.*, 35, 261-70.

Iijima S. (1991). Helical microtubules of grapgitic carbon, *Nature*, 354, 56.

Islas-Blancas, M. E.; Cervantes, J. M.; Vargas-Coronado, R.; Cauich-Rodriguez, J. V.; Vera-Graziano, R. & Martinez-Richa, A. (2001). Characterization of bone cements prepared with functionalized methacrylates and hydroxyapatite. *J Biomater. Sci. Polym. Ed.*, 12, 893-910.

Jain, S. K.; Awasthi, A. M.; Jain, N. K. & Agrawal, G. P. (2005). Calcium silicate based microspheres of repaglinide for gastroretentive floating drug delivery: preparation and in vitro characterization. *J Control Release* 107, 300-9.

Kanakis, J.; Chrissanthopoulos, A.; Tzanetos, N. P.; Kallitsis, J. K. & Dalas, E. (2006). Crystallization of hydroxyapatite on oxadiazole-based homopolymers. *Cryst. Growth Des.* 6, 1547-52.

Kano, S.; Yamazaki, A.; Otsuka, R.; Ohgaki, M.; Akao, M. & Aoki, H. (1994). Application of hydroxyapatite-sol as drug carrier. *Biomed. Mater. Eng.*, 4, 283-90.

Keren, K.; Berman, R. S.; et al. (2003). DNA-templated carbon nanotube field-effect transistor, *Science*, 302, 1380.

Kim, H. W.; Lee, H. H.; Knowles, J. C. (2006). Electrospinning biomedical nanocomposite fibers of hydroxyapaite/poly(lactic acid) for bone regeneration. *J Biomed. Mater. Res. Part A*, 79A, 643-9.

Kim, H. W.; Knowles, J. C. & Kim, H. E. (2004). Hydroxyapatite/poly (epsilon-caprolactone) composite coatings on hydroxyapatite porous bone scaffold for drug delivery. *Biomaterials*, 25, 1279-87.

Kim, I. Y.; Sugino, A.; Kikuta, K. & Ohtsuki , C. (2009). Bioactive composites consisting of PEEK and calcium silicate powders. *J Biomater. Applications* 24, 105-18.

Kithva, P.; Grondahl, L.; Martin, D. & Trau, M. (2010). Biomimetic synthesis and tensile properties of nanostructured high volume fraction hydroxyapatite and chitosan biocomposite films. *J Mater. Chem.* 20, 381-9.

Koga, N.; Nakagoe, Y. Z. & Tanaka, H. (1998). *Thermochimica Acta*, 318, 239.

Kojima, Y.; Kawanobe, A.; Yasue, T. & Arai, Y. (1993). *J Ceram. Soc. Japan* 101, 1145.

Kokubo, T.; Kawai, M.; Kawashita, M.; Yamamoto, K. & Nakamura, T. (2005). Fabrics of polymer fibers modified with calcium silicate for bone substitute. *Key Engineer. Mater.*, 284-286, 775-8.

Lacout, J. L.; Freche, M.; Goncalves, S. & Rodriguez, F. (2009). US6923989.

Lamer, V. K. & Dinegar, R. H. (1950). *J Am. Chem. Soc.*, 72, 4847.

Landi, E.; Tampieri, A.; Celotti, G.; Vichi, L. & Sandri, M. (2004). Influence of synthesis and sintering parameters on the characteristics of carbonate apatite. *Biomaterials*, 25, 1763-70.

Lee, D. D.; Rey, C.; Aiolova, M. &Tofighi, A. (2009).US7517539.

Li,H. J.; Wang, X. B.; Song,Y. L.; Liu, Y. Q.; Li, Q. S.; Jiang, L. & Zhu. D. B. (2001). Super-"amphiphobic" aligned carbon nanotube films. *Angew.Chem.Int.Ed.*, 40, 1743.

Li, H. Y. & Chang, J. (2005). Preparation, characterization and in vitro release of gentamicin from PHBV/wollastonite composite microspheres. *J Controlled Release* 107, 463.

Li, H. Y. & Chang, J. (2005). Preparation, characterization and in vitro release of gentamicin from PHBV/wollastonite composite microspheres. *J Control Release* 107, 463-73.

Lin, J. Y. (2000). Hydrogen storage in nanotubes, *Science*, 287, 1929.

Liu, J. K.; Wu, Q. S. & Ding, Y. P. (2005). Self-assembled synthesis and fluorescent modification of hydroxyapatite nanoribbons spherulites. *Eur. J Inorg. Chem.*, 4145-9.

Lima, R. S.; Khor, K. A.; Li, H.; Cheang, P. & Marple, B. R. (2005). HVOF spraying of nanostructured hydroxyapatite for biomedical applications. *Mater. Sci. Engin. A-Struct. Mater. Prop.s Microstr. Proc.*, 396, 181-7.

Li, Q.; Ding, Y.; Li, F. Q.; Xie, B. & Qian, Y. T. (2002). *J Cryst .Growth 236*, 357.

Li, S. M.; Jia, N.; Zhu, J. F.; Ma, M. G. & Sun, R. C. (2010). Synthesis of cellulose-calcium silicate nanocomposites in ethanol/water mixed solvents and their characterization. *Carbohydr. Polym.* 80, 270-5.

Li, T. & Feng, Y. Q. (2009). Biomimetic fabrication of hydroxyapatite-coated zirconia-magnesia composite and its application in the separation of proteins. *Talanta.* 80, 889-94.

Li, T. T., Lee, J. , Kobayashi, T. & Aoki, H. (1992). Hydroxyapatite coating by dipping method, and bone bonding strength. *J Mater. Sci.: Mater. in Medic.* 7, 355-7.

Li, Y. D.; Wang, J. W.; Deng, Z. X.; Wu, Y. Y.; Sun, X. M. & Yu, D. P. (2001). *J Am. Chem. Soc.* 123, 9904-05.

Lu, X. & Leng, Y. (2005). Theoretical analysis of calcium phosphate precipitation in simulated body fluid. *Biomaterials* 26, 1097-108.

Ma, M. G. & Zhu, J. F. (2009). Solvothermal synthesis and characterization of hierarchically nanostructured hydroxyapatite hollow spheres. *Eur. J Inorg. Chem.*, 5522-6.

Ma, M. G. & Zhu, J. F. (2010). Recent progress on fabrication of calcium-based inorganic biodegradable nanomaterials. *Recent Patents on Nanotechnology*, *4*, 164-70.

Ma, M. G.; Zhu, J. F.; Jia, N.; Li, S. M.; Sun, R. C.; Cao, S. W. & Chen, F. (2010). Rapid microwave-assisted synthesis and characterization of cellulose-hydroxyapatite nanocomposites in *N,N*-dimethylacetamide solvent. *Carbohydr. Res.*, 345, 1046-50.

Ma, M. G.; Zhu, Y. J. & Chang, J. (2008). Solvothermal preparation of hydroxyapatite microtubes in water-*N,N*-dimethylformamide mixed solvents. *Mater. Lett.*, 62, 1642-5.

Ma, M. G.; Zhu, Y. J.; Cheng, G. F. & Huang, Y. H. (2008). Fabrication and characterization of $BaCO_3$ nanostructure. *Materials Letters*, 62, 3110-3113.

Ma, M. G.; Zhu, Y. J.; Zhu, J. F. & Xu, Z. L. (2007). A simple route to synthesis of $BaCO_3$ nanostructures in water/ethylene glycol mixed solvents. *Materials Letters*, 61, 5133-5136.

Ma, M. G.; Zhu, Y. J.; Zhu, J. F. & Cheng, G. F. (2006). Microwave-assisted fabrication and characterization of $BaCO_3$ nanorods, *Chemistry Letters* 35, 10, 1138-1139.

Ma, M. G.; Zhu, Y. J. & Li , S. H. (2009). A simple route to synthesis of $BaCrO_4$ microstructures at room temperature, *Materials Research Bulletin*, 44(2), 288-293.

Ma, M. G.; Jiang, J. X. & Sun, R. C. (2010). Microwave-assisted controlled synthesis of $CaCO_3$ with various biomimetic morphologies using basic additives in polyol. *Advanced Materials Research*, 92, 139-145.

Ma, M. G. & Zhu, Y. J. (2008). Microwave synthesis of $SrCO_3$ one-dimensional nanostructures assembled from nanocrystals using ethylenediamine additive. *Materials Letters*, 62, 2512-2515.

Ma, M. G. & Zhu, Y. J. (2007). A simple route to synthesis of $SrCO_3$ with olive-like and flower-like morphologies, *Journal of Nanoscience and Nanotechnology*, 7, 4552-4556.

Ma, M. Y.; Zhu, Y. J.; Li, L. & Cao, S. W. (2008). Nanostructured porous hollow ellipsoidal capsules of hydroxyapatite and calcium silicate: preparation and application in drug delivery. *J Mater. Chem.*, 18, 2722-7.

Marqusee, J. A. & Ross, J. (1983). *J Chem. Phys.* 79, 373.

Matsumoto, T. &Nakasu, M. (2010). US7687138.

Matsuoka, H.; Akiyama, H.; Okada, Y.; Ito, H.; Shigeno, C.; Konishi, J.; Kokubo, T. & Nakamura, T. (1999). In vitro analysis of the stimulation of bone formation by highly bioactive apatite- and wollastonite-containing glass-ceramic: released calcium ions promote osteogenic differentiation in osteoblastic ROS17/2.8 cells. *J Biomed. Mater. Res.*, 47, 176-88.

McGrath, K. M. (2001),*Adv. Mater.* 13, 989.

McKee, M. D.; Wild, L. M.; Schemitsch, E H. & Waddell, J. P. (2002). The use of an antibiotic-impregnated, osteoconductive, bioabsorbable bone substitute in the treatment of infected long bone defects: early results of a prospective trial. *J Orthop. Trauma*, 16, 622-7.

Miller, R. M. & Tinti, D. S. (1986). *J Lumin.*, 36, 143-147.

Mirtchi, A. A.; Lemaitre, J. & Munting, E. (1990). *Calcium phosphate* cements: *study of* the alfa-*tricalcium* phosphate-dicalcium phosphate-calcite *cements*, *Biomaterials*, 11: 83-8.

Moheno, P. & Pfleiderer, W. (2010). US7662820.

Muller-Mai, C. M.; Voigt, C. & Gross, U. (1990). Incorporation and degradation of hydroxyapatite implants of different surface roughness and surface structure in bone. *Scanning Microsc*, 4, 613-22.

Nagano, M.; Nakamura, T.; Kokubo, T.; Tanahashi, M. & Ogawa, M. (1996). Differences of bone bonding ability and degradation behaviour in vivo between amorphous

calcium phosphate and highly crystalline hydroxyapatite coating. *Biomaterials*, 17, 1771-7.

Nilsson, M.; Fernandez, E.; Sarda, S.; Lidgren, L. & Planell, J. A. (2002). Characterization of a novel calcium phosphate/sulphate bone cement. *J Biomed. Mater. Res.* 61, 600-7.

Oktar, F. N.; Kesenci, K. & Piskin, E. (1999). Characterization of processed tooth hydroxyapatite for potential biomedical implant applications. *Artif Cells Blood Substit Immobil Biotechnol.* 27, 367-79.

Oyane, A.; Kawashita, M.; Nakanishi, K.; Kokubo, T.; Minoda, M.; Miyamoto, T. & Nakamura, T. (2003). *Bonelike apatite formation* on *ethylene*-vinyl alcohol copolymer modified with silane coupling agent and calcium silicate solutions. *Biomaterials* 24, 1729-35.

Owusu, G. & Litz, J. E. (2000). *Hydrometallurgy* 57, 23.

Pacholski, C.; Kornowski, A. & Weller, H. (2002). *Angew. Chem. Int. Ed.* 41, 1188-91.

Penn, R. L. & Banfield, J. F. (1999). *Geochimica et Cosmochimica Acta* 63,1549-57.

Qu, L. T.; Dai, L. M.; Stone, M.; Xia, Z. H. & Wang, Z. L. (2008). Carbon Nanotube Arrays with Strong Shear Binding-On and Easy Normal Lifting-Off. *Science.*, 322, 238.

Rauschmann, M. A.; Wichelhaus, T. A.; Stirnal, V.; Dingeldein, E.;, Zichner, L.; Schnettler, R. & Alt, V. (2005). Nanocrystalline hydroxyapatite and calcium sulphate as biodegradable composite carrier material for local delivery of antibiotics in bone infections. *Biomaterials*, 26, 2677-84.

Riihonen, R.; Nielsen, S.; Vaananen, H. K.; Laitala-Leinonen, T. & Kwon, T. H. (2010). Degradation of hydroxyapatite in vivo and in vitro requires osteoclastic sodium-bicarbonate co-transporter NBCn1. *Matrix Biology*, 29, 287-94.

Rodríguez-Lorenzo, L. M. ; García-Carrodeguas, R.; Rodríguez, M. A.; DeAza, S.; Jime´nez, J.; López-Bravo, A.; Fernandez, M. & Román, J. S. (2009). Synthesis, characterization, bioactivity and biocompatibility of nanostructured materials based on the wollastonite-poly (ethylmethacrylate-co-vinylpyrrolidone) system. *J Biomed.Mater. Res. A* 88, 53-64.

Rudin, V. N.; Komarov, V. F.; Melikhov, I. V.; Minaev, V. V.; Orlov, A. Y. & Bozhevolnov, V.E. (2009). US7169372.

Sakai, H.; Ito, E.; Cai, R. X.; Yoshioka, T.; Kubota, Y.; Hashimoto, K. & Fujishima, A. (1994). Intracellular $Ca^{2+}$ concentration change of T24 cell under irradiation in the presence of $TiO_2$ ultrafine particles. *Biochim. Biophys. Acta* 1201, 259-65

Sato, S.; Koshino, T. & Saito, T. (1998). Osteogenic response of rabbit tibia to hydroxyapatite particle-plaster of paris mixture. *Biomaterials*, 19, 1895-900.

Shi, H.; Qi, L. M.; Ma, J. & Cheng, H. (2003). *J Am. Chem. Soc.* 125, 3450.

Shi, J. J.; Li, J. J.; Zhu, Y. F.; Wei, F. & Zhang, X. R. (2002). *Anal. Chim. Acta* 466, 69.

Shoda, M. & Sugano Y. (2005). Recent advances in bacterial cellulose production. *Biotechnol. Bioproc. Engin.*, 10, 1-8.

Shum, H. C.; Bandyopadhyay, A.; Bose, S. & Weitz, D. A. (2009). Double emulsion droplets as microreactors for synthesis of mesoporous hydroxyapatite. *Chem. Mater.*, 21, 5548-55.

Sotome, S.; Uemura, T.; Tanaka, J.; Kikuchi, M.; Shinomiya, K. & Tateishi, T. (2009). US7494664.

Spek, A. L.; Duisenberg,A. J. M.; Coremans,C. J. M. & der Waals, J. H. (1996). *J Lumin.*, 69, 319-323.

Suchanek, W. L.; Shuk, P.; Byrappa, K.; Riman, R. E.; TenHuisen, K. S. & Janas, V. F. (2002). Mechanochemical hydrothermal synthesis of carbonated apatite powders at room temperature. *Biomaterials*, 23, 699-710.

Sugihara, H.; Anan, T.; Adachi, K.; Baba, A.; Egashira, N. & Nishiguchi, H. (1997). *J Ceram. Soc. Japan* 105, 886-90.

Sugimoto, S. (1978). *J Colloid Interface Sci.* 63, 16.

Sugimoto, T. (1987). *Adv. Colloid Interface Sci.* 28, 65.

Sun, R. X.; Lu, Y. P. & Chen, K. Z. (2009). Preparation and characterization of hollow hydroxyapatite microspheres by spray drying method. *Mater. Sci. Eng. C* 29, 1088-92.

Tarasevich, B. J.; Chusuei, C. C. & Allara, D. L. (2003). Nucleation and growth of calcium phosphate from physiological solutions onto self-assembled templates by a solution-formed nucleus mechanism. *J Phys. Chem. B* 107, 10367-77.

Teo, K. B. K.; Minoux, E.; et al. (2005). Microwave devices- Carbon nanotubes as cold cathodes, *Nature*, 437, 968.

Thian, E. S.; Huang, J.; Vickers, M. E.; Best, S. M.; Barber, Z. H. & Bonfield, W. (2006). Silicon-substituted hydroxyapatite (SiHA): A novel calcium phosphate coating for biomedical applications. *J Mater. Sci.*, 41, 709-17.

Tofighi, A. N. & Rey, C. (2010). US7686239.

Venugopal, A. & Scurrell, M. S. (2003). Hydroxyapatite as a novel support for gold and ruthenium catalysts - Behaviour in the water gas shift reaction. *Appl. Catalys. A-General*, 245, 137-47.

Wahl, D. A. & Czernuszka, J. T. (2006). Collagen-hydroxyapatite composites for hard tissue repair. *Europ. Cells Mater.*, 11, 43-56.

Wang, X.; Zhuang, J.; Peng, Q. & Li Y. D. (2006). Liquid-solid-solution synthesis of biomedical hydroxyapatite nanorods. *Adv. Mater.*, 18, 2031-4.

Wang, H. B.; Lee, J. K.; Moursi, A. & Lannutti, J. J. (2003). Ca/P ratio effects on the degradation of hydroxyapatite in vitro. *J Biomedical Mater. Res. Part A*, 67A, 599-608.

Wang, K. W.; Zhou, L. Z.; Sun, Y.; Wu, G. J.; Gu, H. C.; Duan, Y. R.; Chen, F. & Zhu, Y. J. (2010). Calcium phosphate/PLGA-mPEG hybrid porous nanospheres: A promising vector with ultrahigh gene loading and transfection efficiency. *J Mater. Chem.*, 20, 1161-6.

Wang, L. F.; Sondi, I. & Matijevic. E. (1999). *J Colloid Interf. Sci.* 218, 545.

Wang, W. W. & Zhu, Y. (2005). *J Crystal Growth & Design*, 5, 505-507.

Wei, H.; Shen, Q.; Zhao, Y.; Wang, D. & Xu, D. (2004a). *J Cryst. Growth*, 260, 511.

Wei, H.; Shen, Q.; Zhao, Y.; Wang, D. & Xu, D. (2004b). *J Cryst. Growth*, 260, 545.

Wei, J.; Chen, F. P.; Shin, J. W.; Hong, H.; Dai, C. L.; Su, J. C. & Liu, C. S. (2009). Preparation and characterization of bioactive mesoporous wollastonite -polycaprolactone composite scaffold. *Biomaterials*, 30, 1080-8.

Wei, J.; Heo, S. J.; Li, C. S.; Kim, D. H.; Kim, S. E.; Hyun, Y. T.; Shin, J. W. & Shin, J. W. (2009). Preparation and characterization of bioactive calcium silicate and poly(epsilon-caprolactone) nanocomposite for bone tissue regeneration. *J Biomed. Mater.Res. Part A* 90A, 702-12.

Weiner, S.; Albeck, S. & Addadi, L. (1996). *Chem.Eur.J*, 2, 278.

Wen, C. L.; Guan, S. K.; Peng, L.; Ren, C. X.; Wang, X. & Hu, Z. H. (2009). Characterization and degradation behavior of AZ31 alloy surface modified by bone-like hydroxyapatite for implant applications. *Appl. Surf. Sci.*, 255, 6433-8.

Wenisch, S.; Stahl, J. P.; Horas, U.; Heiss, C.; Kilian, O.; Trinkaus, K.; Hild, A. & Schnettler, R. (2003). In vivo mechanisms of hydroxyapatite ceramic degradation by osteoclasts: Fine structural microscopy. *J Biomedical Mater. Res. Part A* 67A, 713-718.

White, C. T. & Todorov, T. N. (1998). Carbon nanotubes as long ballistic conductors, Nature, 393,240.

Wu, J.; Zhu, Y. J.; Cao, S. W. & Chen, F. (2009). Hierachically nanostructured mesoporous spheres of calcium silicate hydrate: surfactant-free sonochemical synthesis and drug-delivery system with ultrahigh drug-loading capacity. *Adv. Mater.*, 22, 749-53.

Wu, C. Y.; Yu, S. H.; Antonietti, M. (2006). Complex concaved cuboctahedrons of copper sulfide crystals with highly geometrical symmetry created by a solution process. *Chem. Mater.*, *18*, 3599-3601.

Wu, H. C.; Wang, T. W.; Bohn, M. C.; Lin, F. H. & Spector M. (2010). Novel magnetic hydroxyapatite nanoparticles as non-viral vectors for the glial cell line-derived neurotrophic factor gene. *Adv. Funct. Mater.*, 20, 67-77.

Yamaguchi, K.; Hirano, T.; Yoshida, G. & Iwasaki, K. (1995). Degradation-resistant character of synthetic hydroxyapatite blocks filled in bone defects. *Biomaterials*, 16, 983-5.

Yan, Y.; Wu, Q. S.; Li, L. & Ding, Y. P. (2006). *Crystal Growth & Design* 6, 769-773

Yasukawa, A.; Yokoyama, T.; Kandori, K. & Ishikawa, T. (2004). Ion-exchange property and mechanism of magnesium-calcium hydroxyapatite solid solutions. *Colloids Surf. A-Physicochem. Engin. Aspects*. 238, 133-9.

Yaszemski, M.; Currier, B. L.; Jabbari, E. & Lu, L. (2010). US7642300.

Yin, J.; Zou, Z. & Ye, J. (2003). *Chem. Phys. Lett*. 378, 24-28.

Yu, S. H.; Colfen, H. & Antonietti, M. (2003). *Adv.Mater*. 15, 133.

Yu, S. H.; Cölfen, H.; Tauer, K. & Antonietti, M. (2005). Tectonic arrangement of $BaCO_3$ nanocrystals into helices induced by a racemic block copolymer. *Nature Materials 5*, 51-55.

Yuan, Y.; Liu, C. S.; Qjan, J. C.; Wang, J. & Zhang, Y. (2010). Size-mediated cytotoxicity and apoptosis of hydroxyapatite nanoparticles in human hepatoma HepG2 cells. *Biomaterials*, 31, 730-40.

Zeller, A. F. (1981). *Chem. Tech.* 19, 762.

Zhai, J.; Li, H.J.; Li,Y.S.; Li, S.H. & Jiang, L. (2002). *Physics*, 31, 483.

Zhan, J. H.; Lin, H. P. & Mou, C. Y. (2003). *Adv. Mater*. 15, 621-23.

Zhan, Y. J. & Yu, S. H. (2008). Necklace-Like Cu@cross-linked poly(vinyl alcohol) (PVA) core-shell Microncables, *J Am. Chem. Soc.*, *130*, 5650-5651.

Zhang, Z. J.; Sun, J. M.; Cao, H. F.; Zhang, X. Y.; Wang, Y. W. & Yao, Q. (2009). CN101591023.

Zheng, Y. M.; Bai, H.; Huang, Z. B.; Tian, X. L.; Nie, F . Q.; Zhao, Y.; Zhai , J. & Jiang, L. (2010). Directional water collection on wetted spider silk. *Nature* 463, 640-643.

Zhu, J. H.; Yu, S. H.; Xu, A. W. & Cölfen, H. (2009). Biomimetic mineralization of double-stranded and cylindrical helical $BaCO_3$ nanofibres, *Chem. Commun*. 1106-1108.

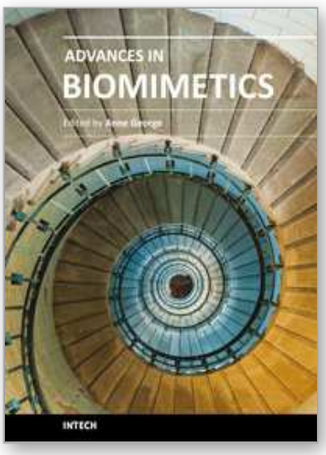


**Advances in Biomimetics**

Edited by Prof. Marko Cavrak

ISBN 978-953-307-191-6
Hard cover, 522 pages
**Publisher** InTech
**Published online** 26, April, 2011
**Published in print edition** April, 2011

The interaction between cells, tissues and biomaterial surfaces are the highlights of the book "Advances in Biomimetics". In this regard the effect of nanostructures and nanotopographies and their effect on the development of a new generation of biomaterials including advanced multifunctional scaffolds for tissue engineering are discussed. The 2 volumes contain articles that cover a wide spectrum of subject matter such as different aspects of the development of scaffolds and coatings with enhanced performance and bioactivity, including investigations of material surface-cell interactions.

**How to reference**

In order to correctly reference this scholarly work, feel free to copy and paste the following:

Ming-Guo Ma and Run-Cang Sun (2011). Biomineralization and Biomimetic Synthesis of Biomineral and Nanomaterials, Advances in Biomimetics, Prof. Marko Cavrak (Ed.), ISBN: 978-953-307-191-6, InTech, Available from: http://www.intechopen.com/books/advances-in-biomimetics/biomineralization-and-biomimetic-synthesis-of-biomineral-and-nanomaterials

INTECH
open science | open minds

**InTech Europe**
University Campus STeP Ri
Slavka Krautzeka 83/A
51000 Rijeka, Croatia
Phone: +385 (51) 770 447
Fax: +385 (51) 686 166
www.intechopen.com

**InTech China**
Unit 405, Office Block, Hotel Equatorial Shanghai
No.65, Yan An Road (West), Shanghai, 200040, China
中国上海市延安西路65号上海国际贵都大饭店办公楼405单元
Phone: +86-21-62489820
Fax: +86-21-62489821

IntechOpen